

1 Assessing branched tetraether lipids as tracers of soil organic carbon 2 transport through the Carminowe Creek catchment (southwest 3 England)

4 Jingjing Guo¹, Miriam Glendell², Jeroen Meersmans³, Frédérique Kirkels¹, Jack J Middelburg¹,
5 Francien Peterse¹

6 ¹Department of Earth Sciences, Utrecht University, 3584 CB Utrecht, the Netherlands

7 ²The James Hutton Institute, Aberdeen, AB15 8QH, UK

8 ³TERRA Teaching and Research Centre, Gembloux Agro-Bio Tech, University of Liege, 5030 Gembloux, Belgium

9 Correspondence to: Jingjing Guo (j.guo@uu.nl)

10 In preparation for submission to: *Biogeosciences*

11 **Abstract.** Soils represent the largest reservoir of organic carbon (OC) on land. Upon mobilisation, this OC is either returned
12 to the atmosphere as carbon dioxide (CO₂), or transported and ultimately locked into (marine) sediments, where it will act as
13 a long-term sink of atmospheric CO₂. These fluxes of soil OC are, however, difficult to evaluate, mostly due to the lack of a
14 soil-specific tracer. In this study, a suite of branched glycerol dialkyl glycerol tetraethers (brGDGTs), which are membrane
15 lipids of soil bacteria, is tested as specific tracers for soil OC from source (soils under arable land, ley, grassland and
16 woodland) to sink (Lake Loe Pool sediments) considering a small catchment located in southwest England (i.e. Carminowe
17 Creek draining into Lake Loe Pool). The analysis of brGDGTs in catchment soils reveals that their distribution is not
18 significantly different across different land use types ($p > 0.05$), and thus does not allow tracing land use-specific soil
19 contributions to Lake Loe Pool sediments. Furthermore, the significantly higher contribution of 6-methyl brGDGT isomers
20 in creek sediments (isomerization ratio (IR) = 0.48 ± 0.10 ; mean \pm s.d., standard deviation; $p < 0.05$) compared to that in
21 catchment soils (IR = 0.28 ± 0.11) indicates that the initial soil signal is substantially altered by brGDGT produced *in situ*.
22 Similarly, the riverine brGDGT signal appears to be overwritten by lacustrine brGDGTs in the lake sedimentary record,
23 indicated by remarkably lower Methylation of Branched Tetraethers (MBT_{5ME} = 0.46 ± 0.02 in creek bed sediment and 0.38
24 ± 0.01 in lake core sediment; $p < 0.05$) and higher Degree of Cyclisation (DC = 0.23 ± 0.02 in creek bed sediment and $0.32 \pm$
25 0.08 in lake core sediment). Thus, in this small catchment, brGDGTs do not allow us to trace soil OC transport.
26 Nevertheless, the downcore changes in the degree of cyclisation and the abundance of isoprenoid GDGTs produced by
27 methanogens in the Lake Loe Pool sediment do reflect local environmental conditions over the past 100 years, and have
28 recorded the eutrophication history of the lake.

29 1 Introduction

30 Globally, around 1500–2000 Pg of carbon is stored in soils in the form of organic matter, which is about two times the
31 amount of carbon in the atmosphere and three times the amount of carbon in vegetation (Janzen, 2004; Smith, 2008). Soil
32 organic carbon (OC) plays an important role in the global carbon cycle, as subtle alterations in the soil OC reservoir may
33 affect the concentration of atmospheric CO₂ and thus influence climate change (Davidson and Janssens, 2006). Atmospheric
34 CO₂ that is fixed by plants through photosynthesis will be stored into soil OC pool, part of which will be transferred to
35 streams and rivers. Upon fluvial discharge, soil OC is buried and locked into the marine or lacustrine sediment, where it will
36 act as a long-term carbon sink. However, instead of a passive pipeline in the carbon cycle, rivers actually represent a
37 dynamic channel, where part of the soil OC is respired back to the atmosphere, and another part may be stored in river bed or
38 lake sediments before reaching the ocean (Cole et al., 2007; Battin et al., 2009; Aufdenkampe et al., 2011). Hence, it is hard
39 to determine the exact amount of soil OC that is transported to the ocean, as the dynamic processes that soil OC undergoes

40 during transport, such as degradation and sequestration, are elusive. This is mostly due to the lack of a specific tracer to
41 distinguish soil OC from the total pool of OC that is also comprised of plant-derived OC, aquatic produced OC, and fossil
42 OC from rock erosion (Blair et al., 2004; Aufdenkampe et al., 2011).

43 To circumvent this problem, lipid biomarkers can be used to trace a specific part of the total OC pool in complex natural
44 environmental systems (Brassell and Eglinton, 1986; Wakeham and Lee, 1993). For example, odd-numbered long chain *n*-
45 alkanes derived from epicuticular plant waxes are widely used to detect the contribution of terrestrial OC to river-dominated
46 marine sediments (Eglinton and Hamilton, 1967; Hedges et al., 1997; Fernandes and Sicre, 2000; Glendell et al., 2018).
47 Similarly, lignin, an abundant biopolymer in vascular plants (Hedges et al., 1997), has been used to trace OC transport along
48 the terrestrial-aquatic continuum by e.g., in the Mississippi River (Goñi et al., 1997; Bianchi et al., 2004), the Amazon River
49 (Hedges et al., 1986, 2000; Feng et al., 2016), and Arctic rivers (Feng et al., 2013). However, these biomarkers are derived
50 from vegetation, which, although land-derived, is not fully representative of soil OC. Thus, in order to specifically trace and
51 quantify the pool of soil OC, another biomarker is needed.

52 Branched glycerol dialkyl glycerol tetraethers (brGDGTs; Fig. 1) are membrane spanning tetraether lipids synthesized by
53 heterotrophic bacteria that thrive in soils and peats all over the world (Weijers et al., 2006a, 2007a; Naafs et al., 2017a).
54 Although the exact producers of these lipids are still unknown, after the detection of a brGDGT and the presumed brGDGT
55 precursor lipid *iso*-diabolic acid in Acidobacterial cultures (Sinninghe Damsté et al., 2011, 2014, 2018), it was assumed that
56 this members of the phylum are the main source organisms of brGDGTs in soils. However, a biological source outside the
57 phylum of Acidobacteria cannot be excluded (Sinninghe Damsté et al., 2018). The occurrence and relative distribution of
58 brGDGTs in a global set of modern surface soils showed that they can have 4 to 6 methyl groups attached to their alkyl
59 backbone, where the degree of branching increases in soils from colder areas. Furthermore, brGDGTs respond to changes in
60 soil pH by forming up to 2 cyclopentane moieties following internal cyclisation, where a higher number of cyclopentane
61 moieties corresponds to a higher soil pH (Weijers et al., 2007a). Initially, a combination of two proxies, the Methylation of
62 Branched Tetraethers (MBT) index and Cyclisation of Branched Tetraethers (CBT) index, was proposed as a proxy to
63 reconstruct the mean air temperature (MAT) and pH of a soil (Weijers et al., 2007a; Peterse et al., 2012). After the
64 identification of novel brGDGT isomers that possess a methyl group at the α and/or ω 6 position rather than at position 5
65 (Fig. 1) and the improvement of the chromatography method used for brGDGT analysis, a modified temperature proxy, the
66 MBT_{SME} was developed (De Jonge et al., 2013, 2014b). Furthermore, the relative abundance of 6-methyl brGDGT isomers,
67 quantified as the Isomerization Ratio (IR), appeared to also relate to soil pH (De Jonge et al., 2014b). Indeed, the analysis of
68 brGDGTs in peat profiles and loess-paleosol sequences has resulted in long-term continental paleotemperature records for
69 various areas, e.g. in deglacial central China (Peterse et al., 2011) and northeast China (Zheng et al., 2017), and western
70 Europe during the early Eocene (Inglis et al., 2017).

71 These brGDGTs have not only been found in soils, but also in coastal marine sediments, where they have been used as the
72 terrestrial end-member in the Branched and Isoprenoid Tetraether (BIT) index that determines the relative contribution of
73 fluvially supplied soil organic matter to marine sediments, where the latter is represented by amounts of the isoprenoid
74 GDGT crenarchaeol (Hopmans et al., 2004). For example, the relative abundance of brGDGTs in a marine sediment core
75 from the Bay of Biscay revealed the early re-activation of European rivers after the last deglaciation (Ménot et al., 2006).
76 Furthermore, brGDGTs stored in continental margin sediments are assumed to represent an integrated climate signal of the
77 nearby land, and have been used as such to generate temperature records of deglacial tropical Africa (Weijers et al., 2007b),
78 and Pliocene North-Western Europe (Dearing Crampton-Flood et al., 2018).

79 Recently, however, brGDGTs have also been found to be produced in aquatic systems such as coastal marine areas (Peterse
80 et al., 2009b; Sinninghe Damsté, 2016), rivers (Kim et al., 2012; Zell et al., 2013, 2014) and lakes (Sinninghe Damsté et al.,
81 2009a; Tierney and Russell, 2009; Loomis et al., 2011, 2014; Schoon et al., 2013; Weber et al., 2015, 2018), which
82 complicates the interpretation of brGDGT-based proxy records. A contribution of *in situ* produced brGDGTs in lakes or on
83 the continental shelf may bias BIT index values towards a more terrestrial signal (e.g. Sinninghe Damsté et al., 2009; De
84 Jonge et al., 2015). Aquatic production in coastal marine areas became first apparent upon comparison of brGDGTs in
85 Svalbard fjord sediments and nearby soils. Whereas the brGDGT signal in the fjord sediments was dominated by compounds
86 containing cyclopentane moieties, soils were characterized by brGDGTs without cyclisation (Peterse et al., 2009b). These
87 substantially different brGDGT signatures in combination with the increasing concentration of brGDGTs towards the open
88 ocean then pointed towards a contribution of *in situ* produced brGDGTs to the fjord sediments. Similarly, brGDGT
89 distributions in lake sediments were found to differ from those in soils surrounding the lake (Sinninghe Damsté et al., 2009;
90 Tierney and Russell, 2009), and generated temperature estimates that severely underestimated actual MAT, mostly due to a
91 high relative abundance of hexamethylated brGDGTs (e.g. Tierney et al., 2010; Loomis et al., 2014; Weber et al., 2015).
92 Finally, the presence of brGDGTs with a polar headgroup still attached in suspended particulate matter (SPM) of several
93 large rivers (Zhang et al., 2012; Zell et al., 2013; De Jonge et al., 2014a) provided strong evidence for aquatic production, as
94 these headgroups are thought to be lost within days after cell death (e.g. Harvey et al., 1986). Notably, these and subsequent
95 studies proposed ways to recognize *in situ* production of brGDGTs in aquatic environments. For example, a high degree of
96 cyclisation is an indicator of brGDGT production in coastal marine zones (Peterse et al., 2009b; Sinninghe Damsté, 2016),
97 for which Sinninghe Damsté (2016) proposed that a weighed number of rings in tetramethylated brGDGTs, quantified as
98 $\#rings_{tetra} > 0.7$ indicates a purely marine source of brGDGTs in continental margin sediments. In rivers, aquatic brGDGTs
99 appear to be characterized by a relatively high contribution of 6-methyl brGDGT isomers, and can be quantified using the IR
100 (De Jonge et al., 2014a).

101 Here we test brGDGTs as tracers for soil OC in Carminowe Creek catchment, a small catchment in southwest England.
102 Previously, an attempt was made to follow OC transport from soil (source) to Lake Loe Pool, the final sink of this
103 catchment, using a combination of stable isotopes of bulk soil OC and plant leaf wax *n*-alkanes as fingerprints for the
104 different vegetation types present in the catchment (i.e. arable land, grassland, ley and woodland) (Glendell et al., 2018).
105 Although most land use types had a distinct *n*-alkane fingerprint, OC derived from arable land and temporary grassland (ley)
106 could not be distinguished (Glendell et al., 2018). Hence, by assuming a primary soil source of the brGDGTs, their analysis
107 in the same samples may contribute to tracing soil OC from different land use types during transport in Carminowe Creek.
108 Moreover, changes in GDGT distributions in a 50 cm long sediment core from Loe Pool may be used to infer changes in soil
109 OC transport dynamics in the catchment over the past century, and potentially couple them to climate or anthropogenic
110 activity related events in the catchment area.

111 **2 Methods**

112 **2.1 Study site and sampling**

113 An overview of the study area and sampling sites is given by Glendell et al. (2018). Briefly, the Carminowe Creek catchment
114 is located in Cornwall in southwest England (50°14' N, 5°16' W), covers an area of around 4.8 km² and varies in elevation
115 from 0 to 80 m above sea level (Fig. 2). It is divided into two subcatchments ('north' and 'south'). The two streams converge
116 around 100 m before their joint outlet, and then flow into a natural freshwater lake Loe Pool (50 ha), which is separated from
117 the Atlantic Ocean by a natural shingle barrier. The mean annual temperature (MAT) and mean annual precipitation (MAP)
118 in this area are approximately 11 °C and 1000 mm year⁻¹, respectively. The land use in this studied catchment is dominated

119 by arable land and temporary grasslands (ley), which are under rotation. The steeper hillslopes are under permanent
120 grassland, and riparian woodland covers the areas near the creek. For this study, 74 surface soil samples (0–15 cm) were
121 collected along 14 hillslope transects, including 31 arable land sites, 14 permanent grassland sites, 24 temporary grassland
122 (ley) sites and 5 woodland sites (Fig. 2). Riverbed sediments were collected at three locations along each of the two
123 tributaries (upstream, midstream and downstream), and one more at the joint outlet. A 50 cm long sediment core was taken
124 in the lake, about 150 m away from the joint outlet. The lake core has been dated by the activity of Caesium-137 (¹³⁷Cs), and
125 it covers the last 100 years (Glendell et al., 2018).

126 2.2 Bulk soil properties

127 Total carbon contents were reported by Glendell et al. (2018). Soil pH was measured in this study using a pH meter in a soil
128 to water ratio of 1:5 (w:v) after shaking for two hours.

129 2.3 GDGT extraction and analysis

130 In total, 74 soil samples, 7 creek bed sediment and 25 lake core sediment samples were analysed for GDGTs. First, 5–7 g of
131 the soils or 3–5 g of the sediments were freeze dried and homogenized, after which they were extracted three times with
132 dichloromethane (DCM) : MeOH (9 : 1, v/v) using an accelerated solvent extractor (ASE 350, Dionex™) at 100 °C and 7.7
133 × 10⁶ Pa to obtain a total lipid extract (TLE). After addition of a known amount of C₄₆ GDGT internal standard (Huguet et
134 al., 2006), the TLEs were dried under a N₂ stream, and then separated into apolar and polar fractions by passing them over
135 an activated Al₂O₃ column using hexane : DCM (9 : 1, v/v) and DCM : MeOH (1 : 1, v/v) respectively. The polar fraction,
136 which contains the GDGTs, was evaporated to dryness under a gentle N₂ stream. After this, the samples were prepared for
137 further analysis by re-dissolving them in a hexane : isopropanol (99 : 1, v/v) mixture, and filtration through a 0.45 μm
138 polytetrafluoroethylene (PTFE) filter.

139 The GDGTs were analysed on an Agilent 1260 Infinity ultra high performance liquid chromatography (UHPLC) coupled to
140 an Agilent 6130 single quadrupole mass spectrometer (MS) with settings according to Hopmans et al. (2016). The GDGTs
141 were separated over two silica Waters Acquity UPLC BEH Hilic columns (1.7 μm, 2.1 mm x 150 mm) preceded by a guard
142 column with the same packing. GDGTs were eluted isocratically at a flow rate of 0.2 ml min⁻¹ using 82% A and 18% B for
143 25 min, followed by a linear gradient to 70% A and 30% B for 25 min, where A = hexane and B = hexane : isopropanol (9 :
144 1, v/v). Sample injection volumes were 10 μL. Ionization of the GDGTs was achieved by atmospheric pressure chemical
145 ionization with the following source settings: gas temperature 200 °C, vaporizer temperature 400 °C, N₂ flow 6 L min⁻¹,
146 capillary voltage 3500 V, nebulizer pressure 25 psi and a corona current of 5.0 μA. By scanning the [M+H]⁺ ions (protonated
147 mass) in selected ion monitoring (SIM) mode, the target compounds were detected at *m/z* 1302 (GDGT-0), 1292
148 (crenarchaeol), 1050 (brGDGT-IIIa), 1048 (brGDGT-IIIb), 1046 (brGDGT-IIIc), 1036 (brGDGT-IIa), 1034 (brGDGT-
149 IIb), 1032 (brGDGT-IIc), 1022 (brGDGT-Ia), 1020 (brGDGT-Ib), 1018 (brGDGT-Ic), with *m/z* 744 for the internal
150 standard. Quantitation was achieved by peak area integration of the [M+H]⁺ ions in Chemstation software B.04.03.

151 2.4 GDGT proxy calculations

152 The roman numerals in following equations refer to the molecular structures of GDGTs in Fig.1. The ratios below were
153 calculated based on the fractional abundances (indicated by using square brackets) of GDGTs. The BIT index was calculated
154 according to Hopmans et al. (2004), and modified to also include 6-methyl brGDGTs:

$$155 \text{ BIT} = \frac{[Ia]+[IIa]+[IIIa]+[IIa']+[IIIa']}{[Ia]+[IIa]+[IIIa]+[IIa']+[IIIa']+[crenarchaeol]} \quad (1)$$

156 The degree of methylation (MBT'_{5ME}) and relative abundances of tetra-, penta-, and hexamethylated brGDGTs were
 157 calculated following De Jonge et al. (2014b) and Sinninghe Damsté et al. (2016):

$$158 \quad MBT'_{5Me} = \frac{[Ia] + [Ib] + [Ic]}{[Ia] + [Ib] + [Ic] + [IIa] + [IIb] + [IIc] + [IIIa]} \quad (2)$$

$$159 \quad \%tetra = \sum[tetramethylated \ brGDGTs] = [Ia] + [Ib] + [Ic] \quad (3)$$

$$160 \quad \%penta = \sum[pentamethylated \ brGDGTs] = [IIa] + [IIb] + [IIc] + [IIa'] + [IIb'] + [IIc'] \quad (4)$$

$$161 \quad \%hexa = \sum[hexamethylated \ brGDGTs] = [IIIa] + [IIIb] + [IIIc] + [IIIa'] + [IIIb'] + [IIIc'] \quad (5)$$

162 Furthermore, the degree of cyclisation (DC) was calculated according to Baxter et al. (2019):

$$163 \quad DC = \frac{[Ib] + 2*[Ic] + [IIb] + [IIb']}{[Ia] + [Ib] + [Ic] + [IIa] + [IIa'] + [IIb] + [IIb']} \quad (6)$$

164 The isomerization ratio (IR) is the ratio between penta- and hexamethylated 6-methyl brGDGTs and the total amount of both
 165 5- and 6-methyl penta- and hexamethylated brGDGTs (De Jonge et al., 2014a):

$$166 \quad IR = \frac{[IIa'] + [IIb'] + [IIc'] + [IIIa'] + [IIIb'] + [IIIc']}{[IIa] + [IIa'] + [IIb] + [IIb'] + [IIc] + [IIc'] + [IIIa] + [IIIa'] + [IIIb] + [IIIb'] + [IIIc] + [IIIc']} \quad (7)$$

167 2.5 Statistical analysis and data visualization

168 The statistical analysis and data visualization were undertaken in R programming (version 3.5.2) (R Core Team, 2018).
 169 Differences in the concentration of brGDGTs and brGDGT-based proxies between different land use types (i.e. arable land,
 170 grassland, ley and woodland), creek bed and lake core sediments were examined by one-way nested ANOVA under
 171 generalized linear model (GLM) followed by post-hoc analysis (Tukey HSD (honest significant difference) test), and were
 172 performed with package ‘car’, ‘carData’ and ‘agricolae’. Differences were considered to be significant at level of $p < 0.05$.
 173 To show how close our sample mean is to the population mean, standard deviation is used (mean \pm s.d.). To examine
 174 whether brGDGT signatures could distinguish soil OC derived from different land use types, principal component analysis
 175 (PCA) was performed with package ‘FactoMineR’ and ‘factoextra’. The box plot and scatter plots were carried out with
 176 package ‘ggplot2’.

177 3 Results

178 3.1 BrGDGTs in soils

179 Most of the brGDGTs were present in all soils. Only brGDGT–IIIc and brGDGT–IIIc' were always below the detection limit
 180 (peak height $> 3x$ baseline), and brGDGT–IIc' was below the detection limit in 13 of the soils (three in arable land, four in
 181 grassland and six in ley). The brGDGTs were dominated by pentamethylated ($49.4 \pm 3.0\%$, mean \pm s.d., standard deviation),
 182 followed by tetramethylated ($39.7 \pm 4.9\%$) and then hexamethylated brGDGTs ($10.9 \pm 2.6\%$; Table 1). The concentration of
 183 brGDGTs ranged between 0.1 and $1.7 \mu\text{g g}^{-1}$ soil, with average of $0.2 \pm 0.1 \mu\text{g g}^{-1}$ soil in arable land, $0.6 \pm 0.4 \mu\text{g g}^{-1}$ soil in
 184 grassland, and $0.4 \pm 0.3 \mu\text{g g}^{-1}$ soil in ley (i.e. the temporary grassland). However, the concentration of brGDGTs in
 185 woodland was $3.0 \pm 1.0 \mu\text{g g}^{-1}$ soil, which was significantly higher than that in other land use types ($0.4 \pm 0.3 \mu\text{g g}^{-1}$ soil; $p <$
 186 0.05 ; Fig. 3a). The C-normalized concentration of brGDGTs in catchment soils ranged between 2.8 to $49.8 \mu\text{g g}^{-1}$ C, $8.1 \pm$
 187 $3.6 \mu\text{g g}^{-1}$ C in arable land, $11.2 \pm 6.7 \mu\text{g g}^{-1}$ C in grassland, $10.5 \pm 4.8 \mu\text{g g}^{-1}$ C in ley, and $37.6 \pm 11.0 \mu\text{g g}^{-1}$ C in woodland
 188 (Fig. 3a; Table 1). The trend of the concentration of brGDGTs along the soil transects was not obvious.

189 BIT index values ranged from 0.57 to 1.00 among land use types (Fig. 3b), with an average value of 0.96 ± 0.03 in
190 woodland, 0.90 ± 0.12 in ley, 0.88 ± 0.14 in grassland and 0.83 ± 0.09 in arable land (without significant differences, $p >$
191 0.05). However, the BIT values increased from hillslope to downslope along several transects in north catchment, while the
192 BIT values show no clear trends in south catchment (Fig. A1). The MBT'_{5ME} ranged from 0.37 to 0.71 and was mostly
193 similar between all land use types (0.48 ± 0.04 ; $p > 0.05$; Fig. 3c; Table 1). The degree of cyclisation between land use types
194 was similar ($DC = 0.23 \pm 0.13$; Fig. 3d; Table 1; $p > 0.05$), likewise, the IR ranged from 0.10 to 0.60 (0.28 ± 0.01 on
195 average; Fig. 3e; Table 1; $p > 0.05$), without clear trend along the soil transects. However, four transects in the north
196 catchment have on average significantly higher IR values (> 0.36) than the other transects in the catchment (0.24 ± 0.09 ; $p <$
197 0.05 ; Fig. A1). In general, the IR increases with increasing soil pH in the catchment ($r^2 = 0.36$, $p < 0.001$).

198 **3.2 BrGDGTs in creek bed sediments**

199 All brGDGT compounds were detected in creek bed sediments, except for in the upstream site from north catchment, where
200 brGDGT–IIIc' was below detection limit. The brGDGTs in creek bed sediments were dominated by pentamethylated
201 brGDGTs ($45.0 \pm 0.7\%$), followed by tetramethylated brGDGTs ($30.1 \pm 4.5\%$), and hexamethylated brGDGTs ($24.9 \pm$
202 4.7%) (Table 1). The C-normalized concentration of brGDGTs in creek bed sediments was $34.7 \pm 17.4 \mu\text{g g}^{-1} \text{C}$ on average
203 (Fig. 3a; Table 1), where the concentration increased from $32.7 \mu\text{g g}^{-1} \text{C}$ to $57.0 \mu\text{g g}^{-1} \text{C}$ downstream in north catchment,
204 and from $14.3 \mu\text{g g}^{-1} \text{C}$ to $25.2 \mu\text{g g}^{-1} \text{C}$ downstream in south catchment, reaching a maximum value of $59.3 \mu\text{g g}^{-1} \text{C}$ at the
205 outlet (Fig. 5a). The concentration of brGDGTs in creek bed sediments was higher than that in soils under any land use
206 types, except for woodland ($9.6 \pm 4.9 \mu\text{g g}^{-1} \text{C}$; Fig. 3a; Table 1).

207 The BIT values for creek sediments were on average 0.90 ± 0.06 (Fig. 3b; Table 1). The MBT'_{5ME} was relatively constant
208 between 0.44 and 0.49, with an average of 0.46 ± 0.02 . The DC ranged from 0.21 to 0.25 in the creek sediments with an
209 average of 0.23 ± 0.02 (Fig. 3e; Table 1). The IR was relatively invariable with an average of 0.48 ± 0.10 (Fig. 3e; Table 1).
210 The brGDGT-based proxies for creek bed sediments were similar to those for soils, except for the IR, which was higher than
211 that in soils under any land use types (0.28 ± 0.11 ; Fig. 3; Table 1).

212 **3.3 BrGDGTs in Lake Loe Pool sediment core**

213 All brGDGTs were detected in the lake sediment core, except at 20 cm depth, where brGDGT–IIIc' was below the detection
214 limit. The brGDGTs in the lake sediments were mainly dominated by pentamethylated brGDGTs ($50.2 \pm 1.8\%$), followed by
215 tetramethylated brGDGTs ($28.9 \pm 0.7\%$), and hexamethylated brGDGTs ($21.0 \pm 1.4\%$; Table 1). The amount of brGDGTs in
216 lake core sediment ranged from 19.9 to $48.0 \mu\text{g g}^{-1} \text{C}$ (Fig. 3a; Table 1). The brGDGT concentration in the surface sediment
217 (0–2 cm), of $37.7 \mu\text{g g}^{-1} \text{C}$, which was about 1.6 times lower than that in the creek sediment at the outlet (Fig. 5a), increased
218 to a maximum of $48.0 \mu\text{g g}^{-1} \text{C}$ around 11 cm depth, and then decreased to a minimum of $19.9 \mu\text{g g}^{-1} \text{C}$ at 23 cm depth (Fig.
219 6b). The concentration of GDGT-0 ranged between $9.0 \mu\text{g g}^{-1} \text{C}$ and $27.1 \mu\text{g g}^{-1} \text{C}$ with an average of $17.4 \pm 6.0 \mu\text{g g}^{-1} \text{C}$,
220 concentration of crenarchaeol ranged from $0.6 \mu\text{g g}^{-1} \text{C}$ to $1.4 \mu\text{g g}^{-1} \text{C}$ with an average of $1.0 \pm 0.2 \mu\text{g g}^{-1} \text{C}$ in the lake
221 sediment core. In general, the concentration of brGDGTs in lake core ($34.0 \pm 8.7 \mu\text{g g}^{-1} \text{C}$; Table 1) was similar with that in
222 river and in woodland, while it was significantly higher than the brGDGTs in soils except for the woodland ($9.6 \pm 4.9 \mu\text{g g}^{-1}$
223 C ; $p < 0.05$; Fig. 3a; Table 1).

224 The BIT values for the lake sediment core were rather uniform, varying between 0.95 and 0.97 (Fig.3b). Similarly, the
225 values of MBT'_{5ME} along the lake core ranged only between 0.36 and 0.39. The MBT'_{5ME} of 0.37 for the lake surface
226 sediment was significantly lower than that in creek bed sediment (0.46 ± 0.02 ; $p < 0.05$; Fig 3c; Fig. 5b). Conversely, the DC
227 in the lake surface sediment was 0.39, which was significantly higher than that in creek bed sediment (0.23 ± 0.02 ; $p < 0.05$;

228 Fig. 3d; Fig. 5b). The average value of DC for the lake core sediments was 0.32 ± 0.08 . The DC increased from the surface
229 to a maximum value (0.44) at around 10 cm depth, and then decreased with slight fluctuations to 0.22 at 43 cm depth (Fig.
230 6c). The IR was constant downcore (0.32 ± 0.01 on average; Fig. 3e; Table 1) and was significantly lower than that in creek
231 bed sediment ($p < 0.05$; Fig. 3e).

232 4 Discussion

233 4.1 Spatial variation of brGDGT signals in catchment soils

234 Spatial variations in the relative distribution of brGDGTs in all catchment soils were first evaluated by performing principal
235 component analysis (PCA) using the fractional abundances of the 13 major brGDGTs detected. The first two principal
236 components (PCs) explain 65.2% of the variance in the dataset. PC1 describes 49.5% of the variance, and separates acyclic
237 brGDGT-Ia and brGDGT-IIa from all the other brGDGTs (Fig. 4a). In line with this observation, PC1 has a strong positive
238 relationship with the degree of cyclisation of brGDGTs in the soils ($r^2 = 0.97$; Fig. 4c). PC2 describes another 15.7% of the
239 variance, and separates tetramethylated brGDGTs as well as most of the 6-methyl brGDGTs from the majority of the 5-
240 methyl penta- and hexamethylated brGDGTs. As a result, PC2 is negatively correlated with MBT'_{SME} ($r^2 = 0.49$; Fig. 4d) as
241 well as the IR ($r^2 = 0.58$; Fig. 4e) in soils. Despite the clear relation of the first two PCs with the degree of cyclisation and the
242 degree of methylation, respectively, the position of the soils in the PCA diagram reveals that different land use types are
243 largely overlapping (Fig. 4b). Indeed, the brGDGTs proxies for different land use types are not significantly different ($p >$
244 0.05 ; Fig. 3), making it difficult to distinguish the provenance of soil OC solely based on brGDGT signatures.

245 Indeed, previous work has also shown that brGDGT distributions are not primarily affected by land use. For example,
246 brGDGTs in soils along an altitudinal transect in the Ethiopian highlands revealed that brGDGTs mainly reflect the decrease
247 in temperature with increasing elevation, regardless of drastic changes in land use along the transect (Jaeschke et al., 2018).
248 However, other studies report that vegetation cover does exert a great influence on brGDGT signatures in soils from
249 Minnesota and Ohio, USA (Weijers et al., 2011), around Lake Rotsee, Switzerland (Naeher et al., 2014), in the Tibetan
250 Plateau (Liang et al., 2019), and paddy and upland soils from subtropical (China and Italy) and tropical (Indonesia,
251 Philippines and Vietnam) areas (Mueller-Niggemann et al., 2016). The explanations for the similar distribution of brGDGTs
252 under different land use types in the Carminowe Creek catchment could be the rotation and ploughing in land use in
253 combination with the turnover time of brGDGTs. Although the soil bacterial community composition is generally different
254 across distinct land use types (Fierer and Jackson, 2006; Steenwerth et al., 2003), the regular rotation (generally less than 5
255 years) of arable land and temporary grassland (ley) in the catchment (Glendell et al., 2018) may create a mixed bacterial
256 community under all vegetation types. Beyond vegetation, regular ploughing as applied across the Carminowe catchment
257 soils (arable land and ley) is recognized to have a more dominant, long-last effect on microbial communities (Drenovsky et
258 al., 2010). Moreover, brGDGTs in terrestrial environments have a relatively long turnover time (ca. 18 years in soils
259 (Weijers et al., 2010), and up to 40 years in peat (Huguet et al., 2017)), especially when compared to the cropland rotation
260 time. Taken together, these factors may contribute to the relatively similar brGDGT signal in all soils in the Carminowe
261 catchment, further limiting the variation in brGDGT signals in catchment soils.

262 Some spatial trends are visible in spite of the overall comparable brGDGT signals across the catchment (Fig. A1), which
263 may be explained by variations in other environmental factors than land use or vegetation. Mean air temperature and soil pH
264 have been shown to be the main factors controlling the distribution of brGDGTs in soils worldwide (Weijers et al., 2007a;
265 Peterse et al., 2012; De Jonge et al., 2014b). However, in the small (ca. 4.8 km²) Carminowe Creek catchment, the annual
266 mean air temperature is practically the same for all soils. Similarly, the range in soil pH is relatively small among different
267 land use types (from 5.4 ± 0.3 in woodland to 6.6 ± 0.1 in arable land; Table 1), which makes it difficult to separate brGDGT

268 signals based on these parameters. Additionally, the soil water content (SWC) has been shown to affect the distribution and
269 abundance of brGDGTs in soils, either directly by changing the microbial community, or indirectly by altering soil
270 temperature, soil pH, or soil oxygen content (Dirghangi et al., 2013; Menges et al., 2014; Dang et al., 2016). The SWC
271 positively correlates with the abundance of brGDGTs in soils from Qinghai-Tibetan Plateau (Wang et al., 2013), as well as
272 in soils along an aridity transect in the USA (Dirghangi et al., 2013). Moreover, the degree of methylation of 6-methylated
273 brGDGTs is sensitive to the SWC, especially in semi-arid and arid regions (Dang et al., 2016). Although MAP is also the
274 same for the whole catchment, the subtle altitudinal differences in this small creek catchment (i.e. 0-80 m above sea level)
275 may result in an increase in SWC from hilltop to downslope. This would introduce just enough variability in SWC to explain
276 some of the trends in brGDGT signals along hillslope transects. In the north catchment, the BIT index values gradually
277 increase from the presumably better aerated soils at the hilltops towards the wetter soils closer to the creek (Fig. A1). The
278 increase is > 0.3 for Transects 1 and 8, but also Transects 2, 3, and 7 show an increase in BIT values downslope, albeit to a
279 smaller degree (0.17, 0.19, and 0.04, respectively; Table A1). The change in BIT index values is driven by both an increase
280 in the amount of brGDGTs and a slight decrease in crenarchaeol concentrations with the presumed increase in SWC
281 downslope, similar to previous findings (Dirghangi et al., 2013; Wang et al., 2013; Menges et al., 2014). The trend in BIT is
282 likely enhanced by the (minor) change in soil pH along Transects 1 and 8 (from 6.2 to 6.1 along Transect-1 and from 6.6 to
283 5.7 along Transect-8), which may influence the BIT index as a result of the generally positive relation of crenarchaeol
284 concentrations and a negative relation of brGDGT concentrations with increasing soil pH (Weijers et al., 2006b; Peterse et
285 al., 2010). Nevertheless, these trends in the BIT index are visible in five of the transects and only occur in the north part of
286 the catchment.

287 Interestingly, the IR is also significantly higher in soils along four transects in north catchment (all > 0.36 averagely for
288 Transects 1, 2, 7, and 8) compared to the average IR value for the rest of the transects in the entire catchment (0.24 ± 0.09 ; p
289 < 0.05). The majority of the sites with higher IR are in cropland, except for those in the Transect-1, which is under grassland
290 (Fig. A2). Although a relative increase in 6-methyl brGDGTs has been linked to higher soil pH in the global soil dataset (De
291 Jonge et al., 2014b), this relation is not so strong in the soils from the Carminowe creek catchment ($r^2 = 0.36$, $p < 0.001$),
292 likely due to the relatively minor range and variation in soil pH (from 5.4 ± 0.3 to 6.6 ± 0.1). Nevertheless, the soils with
293 high IR values in the north catchment also have pH values > 6.0 with an average value of 6.6 ± 0.1 .

294 4.2 Tracing brGDGTs from soils to creek bed sediments

295 Based on the similar brGDGT signatures for soils under different land use types, these compounds cannot be used to trace
296 back the exact source of the soil OC after mobilisation and transport throughout the catchment. However, the concentration
297 and general soil signature of the brGDGTs can be compared with those in creek bed sediments to trace the transfer of OC
298 from the soils into the creeks. The C-normalized concentration of brGDGTs in the creek sediments is higher than that in
299 most of the soils ($34.7 \pm 17.4 \mu\text{g g}^{-1} \text{C}$ and $9.6 \pm 4.9 \mu\text{g g}^{-1} \text{C}$ respectively), except for those in the woodland soils at the
300 riverbanks ($37.6 \pm 11.0 \mu\text{g g}^{-1} \text{C}$; Table 1). Thus, purely based on the concentration, this suggests that brGDGTs in the creek
301 would be primarily derived from the woodland, which also appeared to be the main source of *n*-alkanes in creek bed
302 sediment (Glendell et al., 2018). However, when looking at the relative distribution of the brGDGTs, the percentage of
303 hexamethylated brGDGTs in creek sediments is higher than that in soils ($24.9 \pm 1.8\%$ and $10.9 \pm 0.3\%$, respectively),
304 whereas the percentage of tetramethylated brGDGTs is lower than in soils ($30.1 \pm 1.7\%$ and $39.7 \pm 0.6\%$, respectively; Table
305 1). Furthermore, brGDGTs in creek sediments have a significantly higher IR (i.e. 0.48 ± 0.04) than soils under any of the
306 land use types (0.28 ± 0.01 on average in the catchment; $p < 0.05$; Fig. 3e; Table 1). This is clearly reflected in the PCA,
307 which separates the creek sediments from both the soils and lake sediments on PC2 that is associated with the IR (Fig. 4e).
308 The higher IR in the creek bed sediments can be explained by a contribution of aquatically (i.e. *in situ*) produced 6-methyl

309 brGDGTs. Similar contributions of 6-methyl brGDGTs, and thus higher IR, were also observed in suspended particulate
310 matters from the Yenisei River (De Jonge et al., 2014a), and upstream of the Iron Gates in the Danube River, where the
311 higher IR was coupled to in-river production facilitated by the lower flow velocity and decreased turbidity of the river water
312 (Freymond et al., 2017). Hence, the significantly higher IR in combination with the higher C-normalized concentrations of
313 brGDGTs in the Carminowe creek sediments suggests that the brGDGT signal is mainly aquatic.

314 In attempt to further prove the riverine *in situ* production of brGDGTs, we roughly estimate the minimum amount of 6-
315 methyl brGDGTs that needs to be produced in the creek in order to reach the higher IR. We hereby assume that the
316 brGDGTs derived from woodland soils are completely transferred into creek without any degradation. Thus, the
317 concentration of 6-methyl brGDGTs in the creek sediments [$6\text{-me}_{\text{creek}}$] resembles the sum of the average concentration of 6-
318 methyl brGDGTs in woodland soils [$6\text{-me}_{\text{woodland}}$] and those produced *in situ* [$6\text{-me}_{\text{in situ}}$]. The minimum amount of 6-methyl
319 brGDGTs produced *in situ* can then be calculated using the brGDGT-concentration-weighted IR for creek sediments (IR_{creek}
320 = 0.47) and the following equation (Eq. 8).

$$321 \quad \text{IR}_{\text{creek}} = \frac{[6\text{-me}_{\text{creek}}]}{[5\text{-me}_{\text{creek}}] + [6\text{-me}_{\text{creek}}]} = \frac{[6\text{-me}_{\text{woodland}}] + [6\text{-me}_{\text{in situ}}]}{[5\text{-me}_{\text{creek}}] + [6\text{-me}_{\text{woodland}}] + [6\text{-me}_{\text{in situ}}]} \quad (8)$$

322 Solving this equation results in a minimum amount of $7.4 \mu\text{g g}^{-1}$ C 6-methyl brGDGTs that needs to be additionally
323 produced in the creek to reach the higher IR. This accounts for 65% of the total amount of 6-methyl brGDGTs in the creek
324 bed sediment that we measured. Considering a mixture of all soils rather than only woodland as source for soil-derived
325 brGDGTs in the creek results in the *in situ* production of $9.3 \mu\text{g g}^{-1}$ C 6-methyl brGDGTs, corresponding to 81% of the 6-
326 methyl brGDGT pool in the creek bed sediments. This implies that the initial soil brGDGT signal is rapidly overprinted by a
327 riverine *in situ* signal upon entering the creek. Only the IR for the downstream site in the northern creek approaches that of
328 the adjacent soil (IR = 0.30 in the creek bed sediment and 0.38 ± 0.07 for Transect-7; Fig. A2), and may be explained by its
329 use as arable land (Fig. 5a), which involves regular ploughing and subsequent soil mobilisation and implies a temporary,
330 local overprint.

331 The absence of a clearly recognizable soil brGDGT signal in the creek bed sediments may be further explained by the
332 relatively limited input of soil material into the creek. So far, river systems that have shown to transport a soil-derived
333 brGDGT signal are either characterized by a distinct rainy season (e.g. the Congo River (Weijers et al., 2007b; Hemingway
334 et al., 2017) or the Amazon River (Kim et al., 2012)), or have experienced a recent episode of extreme rainfall (e.g. the
335 Danube River, >100 mm in 3 days causing a 100-year flood event, (Freymond et al., 2017) or the Rhône River, with heavy
336 rainfall during sampling (Kim et al., 2015)). The Carminowe creek area does not have a clear rainy season, and is further
337 characterized by its limited relief. Hence, the relatively minor input of soil-derived brGDGTs seems to be easily overprinted
338 by riverine *in situ* production. Alternatively, the soil-derived brGDGTs could be preferentially degraded in an aquatic
339 environment as a result of priming effect (Bianchi, 2011), which would lead to a signature that is dominated by brGDGTs
340 that are produced *in situ*.

341 4.3 Sources of brGDGTs in the sediments of Lake Loe Pool

342 In theory, rivers would transport soil-derived OC together with any aquatic OC produced along the way. Once discharged, in
343 this case into a lake, the OC would settle and then be buried into the sediments where it would act as a long-term sink of OC.
344 However, the soil brGDGT signal cannot be recognized in the sediments from Loe Pool since it is already lost upon entering
345 the Carminowe creek. Indeed, the PCA of the relative distributions of brGDGTs indicates that lake sediments plot
346 completely separated from both the soils and creek sediments, mostly due to a higher relative abundance of GDGT-IIIa (Fig.
347 4a, b). As a result, the $\text{MBT}^{5\text{ME}}$ is significantly lower in Loe Pool sediments (0.38 ± 0.00) compared to in the creek bed

348 sediments (0.46 ± 0.01 ; $p < 0.05$) and soils (0.48 ± 0.01 ; $p < 0.05$; Fig. 5b; Table 1). Furthermore, the DC is significantly
349 higher in lake sediments than in both soil and creek bed sediments (0.32 ± 0.02 , 0.23 ± 0.01 and 0.23 ± 0.01 , respectively; p
350 < 0.05 ; Fig. 3d; Table 1). The distinct brGDGT signature of the lake sediments suggests that brGDGTs in the lake again are
351 significantly altered compared to those in the soils and creek sediments. This implies that the riverine brGDGT signal is
352 either replaced or overwritten in the lake.

353 Lacustrine *in situ* production of brGDGTs has been reported in other studies (Sinninghe Damsté et al., 2009; Tierney and
354 Russell, 2009; Buckles et al., 2014; Loomis et al., 2011, 2014a; Weber et al., 2015, 2018; Miller et al., 2018). However,
355 there are no generally recognized indicators (yet) to identify lacustrine brGDGT production, although several studies
356 reported a “cold bias” while attempting to reconstruct the mean air temperature (MAT) based on brGDGTs in lake sediments
357 using a soil-based transfer function (Tierney et al., 2010). In a study on East African lakes, this cold bias was linked to a
358 large *in situ* contribution of brGDGT-IIIa (Tierney et al., 2010), similar to in Loe Pool. However, the East African lake
359 dataset was generated using the ‘old’ chromatography method that does not separate 5-methyl and 6-methyl brGDGTs. A
360 recent study that has re-analysed the East African Lake dataset indicates that the presumed contribution of GDGT-IIIa
361 mainly consists of brGDGT-IIIa' (Russell et al., 2018), which is less prominent in lake Loe Pool. Although the identity of
362 brGDGT-producer(s) in lakes still remain(s) elusive, a recent study from the stratified Lake Lugano (Switzerland) showed
363 that the majority of the brGDGTs are produced in the lower, anoxic part of the water column rather than in the sediment
364 (Weber et al., 2018). Furthermore, the combination of brGDGT analysis with molecular biological methods revealed that
365 brGDGTs appeared to be produced by multiple groups of bacteria thriving under different redox regimes in this stratified
366 lake. Specifically, brGDGT-IIIa occurred in the entire water column and continuously increased with depth, whereas
367 brGDGT-IIIa' was mainly produced in the upper, oxygenated part of water column (Weber et al., 2018). Extrapolating the
368 ecological niches of brGDGT production in Lake Lugano to Loe Pool we can speculate that brGDGT-IIIa, which is
369 dominating the brGDGT signal in the Loe Pool sediments, is mostly produced in the lake during summer, when the
370 eutrophic state of the lake may seasonally cause the anoxic conditions favourable for its (i.e. brGDGT-IIIa) production.
371 However, our dataset does not allow to further pinpoint the time and depth of lacustrine brGDGT production, or whether
372 brGDGTs are solely produced in the water column of Loe Pool or also in the lake sediment.

373 **4.4 Reconstructing local environmental changes based on GDGTs in Loe Pool lake sediments**

374 Downcore variations in the brGDGT distribution of Lake Loe Pool sediments may provide information on past
375 environmental changes in the catchment, in spite of the lacustrine *in situ* production in Lake Loe Pool. The 50 cm deep
376 sediment core covers about the last 100 years based on ^{137}Cs activity (Glendell et al., 2018). The peak activity correlated
377 with bomb testing in the 1960s was detected at 26 cm depth (Fig. 6a), which can thus be linked to 1963 (Glendell et al.,
378 2018).

379 The C-normalized concentration of brGDGTs starts to increase around 23 cm, reaching a maximum concentration of $48.0 \mu\text{g}$
380 $\text{g}^{-1} \text{C}$ at 11 cm depth (Fig. 6b). The increased brGDGT concentrations coincide with an increase in the degree of cyclisation
381 (Fig. 6c), which generally responds to a change in pH, where more cyclopentane moieties correspond to a higher pH
382 (Weijers et al., 2007a; Schoon et al., 2013). According to historical records, agriculture and anthropogenic perturbations
383 such as mining and urban pollution intensified in the 1960s (~ 26 cm depth), which increased the input of soil and nutrients
384 into Lake Loe Pool (Coard et al., 1983), and resulted in eutrophication (i.e. blooms of cyanobacteria and algae) since at least
385 1986 (~ 23 cm depth) (O'Sullivan, 1992; Flory and Hawley, 1994). Earlier studies have also recognized an increased use of
386 farmyard manures and septic tanks at this time in the nitrogen isotopic composition of the lake sediments, and have detected
387 higher inputs of terrestrial organic material resulting from intensified farming practices and a higher erosion rate during the
388 1960s to 1980s based on ratios of aquatic- and terrestrial-derived plant waxes (Glendell et al., 2018). Thus, the high brGDGT

389 concentrations and DC in the sediments likely reflect the eutrophic conditions of the lake resulting from the increased
390 nutrient input to the lake (Coard et al., 1983). The DC has then recorded the increase in lake water pH associated with
391 eutrophication, whereas brGDGT concentrations express increased aquatic production. Due to remediation measures taken
392 by the local government in 1996 (~ 12 cm depth), the eutrophication has reduced over the past twenty years (Glendell et al.,
393 2018). The partial recovery of the lake has likely resulted in a return to lower lake water pH, as manifested in the decrease in
394 the DC from ~ 10 cm depth upwards (Fig. 6c).

395 The process of eutrophication and subsequent recovery can also be recognized in the ratio between GDGT-0 and
396 crenarchaeol, which are isoprenoidal GDGTs produced by Archaea. Crenarchaeol is produced by ammonia oxidizing
397 Thaumarchaeota (Sinninghe Damsté et al., 2002) in aquatic environments (Schouten et al., 2000; Powers et al., 2004) and to
398 a lesser extent also in soils (Weijers et al., 2006a), whereas GDGT-0 is a membrane lipid that occurs in all major groups of
399 Archaea, but is indicative of methanogens and thus anaerobic conditions, with a typical ratio of GDGT-0 and crenarchaeol >
400 2 (Blaga et al., 2009). The ratio of GDGT-0/crenarchaeol in the sediments of Loe Pool is > 2 throughout the entire core, and
401 ranges between 10.9 and 24.3, indicating that at least the bottom waters of the lake have been (seasonally) anoxic over the
402 past 100 years (Fig. 6d), although the isoGDGTs may potentially be produced in deeper sediments. The ratio reaches its
403 maximum at 16 cm depth, suggesting that eutrophic conditions and bottom water anoxia were most severe around this time.
404 The recovery of the lake after the remediation measures is again reflected in the return to pre-1960 values at ~ 10 cm depth
405 (Fig. 6d).

406 **5 Conclusions**

407 In this study, brGDGTs were tested as a tracer for the transport of soil OC from different vegetation and land use types from
408 source (soil) to sink (lake Loe Pool) in the Carminowe Creek catchment with the aim to reconstruct the provenance of the
409 soil OC in lake Loe Pool sediments over time. Unfortunately, brGDGT signatures in the catchment soils are not distinct for
410 land use types, indicating that other environmental parameters have a larger influence on the distribution of brGDGTs in
411 these soils. Although temperature and precipitation can be considered equal for all soils due to the small size of the
412 catchment, changes in BIT index values and the relative contribution of 6-methyl brGDGTs along a part of the hilltop
413 transects indicate that soil water content (SWC) may exert a control on brGDGT signals, assuming that SWC increases
414 downslope. The regular rotation of cropland in this catchment and the relative long turnover time of brGDGTs in soils could
415 be another reason to explain the limited spatial variation in brGDGT signals.

416 Comparison of the soil-derived brGDGT signals to that of creek bed sediments reveals that the soil brGDGT signal is almost
417 completely overprinted by aquatically produced brGDGTs, indicated by a substantially higher fractional abundance of 6-
418 methyl brGDGTs in the creek. Upon discharge into the lake, the creek brGDGT signal is replaced by and/or mixed with a
419 lacustrine *in situ* produced brGDGT signal, which is characterized by a relatively higher DC and lower MBT'_{5ME}, as well as a
420 specifically high fractional abundance brGDGT-IIIa. Despite regular ploughing of the land, the absence of a profound rainy
421 season and limited relief likely limits the degree of soil mobilisation necessary to transfer the soil-derived brGDGT signal to
422 the lake sediments in the modern system. Still, downcore variations in GDGT distributions in the sediments of Loe Pool do
423 reflect local environmental conditions over the past 100 years. The degree of cyclisation of brGDGTs as well as the ratio of
424 isoprenoidal GDGT-0 and crenarchaeol produced by Archaea trace the historical record of lake eutrophication induced by
425 increased nutrient input from intensified agricultural activity in the catchment during the 1960s to 1980s, and its recovery
426 after measures taken by the owner since 1996. Our study shows that GDGTs in sedimentary archives are good recorders of
427 past environmental and land management (e.g. agricultural intensification, increased fertilizer use) change, although the
428 ability of brGDGTs to trace soil OC along a soil-aquatic continuum requires a higher degree of soil mobilisation.

429 **Data availability**

430 All data are available in the Supplementary Information.

431 **Author Contribution**

432 J.M., F.K., and F.P designed the study, M.G. and J.M. collected the sample material. J.G. conducted the biomarker analysis
433 and interpreted the data under supervision of F.P. and J.J.M, J.G. and F.P wrote the paper with input from all co-authors.

434 **Competing interests**

435 The authors declare that they have no conflict of interest.

436 **Acknowledgements**

437 This study was supported financially by NWO Veni grant #863.13.016 to Francien Peterse. Desmond Eefting and Klaas
438 Nierop (UU) are acknowledged for technical support. Dr. R. Sparkes and anonymous reviewers are thanked for their
439 comments, which helped to improve this manuscript.

440 **References**

- 441 Aufdenkampe, A. K., Mayorga, E., Raymond, P. A., Melack, J. M., Doney, S. C., Alin, S. R., Aalto, R. E. and Yoo, K.:
442 Riverine coupling of biogeochemical cycles between land, oceans, and atmosphere, *Front. Ecol. Environ.*, 9(1), 53–60,
443 doi:10.1890/100014, 2011.
- 444 Battin, T. J., Luysaert, S., Kaplan, L. A., Aufdenkampe, A. K., Richter, A. and Tranvik, L. J.: The boundless carbon cycle,
445 *Nat. Geosci.*, 2(9), 598–600, doi:10.1038/ngeo618, 2009.
- 446 Baxter, A. J., Hopmans, E. C. and Russell, J. M.: ScienceDirect Bacterial GMGTs in East African lake sediments : Their
447 potential as palaeotemperature indicators, , 259, 155–169, doi:10.1016/j.gca.2019.05.039, 2019.
- 448 Bianchi, T. S., Filley, T., Dria, K. and Hatcher, P. G.: Temporal variability in sources of dissolved organic carbon in the
449 lower Mississippi River, *Geochim. Cosmochim. Acta*, 68(5), 959–967, doi:10.1016/j.gca.2003.07.011, 2004.
- 450 Bianchi, T. S.: The role of terrestrially derived organic carbon in the coastal ocean: A changing paradigm and the priming
451 effect, *Proc. Natl. Acad. Sci. U. S. A.*, 108(49), 19473–19481, doi:10.1073/pnas.1017982108, 2011.
- 452 Blaga, C. I., Reichart, G. J., Heiri, O. and Sinninghe Damsté, J. S.: Tetraether membrane lipid distributions in water-column
453 particulate matter and sediments: A study of 47 European lakes along a north-south transect, *J. Paleolimnol.*, 41(3), 523–540,
454 doi:10.1007/s10933-008-9242-2, 2009.
- 455 Blair, N. E., Leithold, E. L. and Aller, R. C.: From bedrock to burial: the evolution of particulate organic carbon across
456 coupled watershed-continental margin systems, *Mar. Chem.*, 92(1–4), 141–156, doi:10.1016/j.marchem.2004.06.023, 2004.
- 457 Brassell, S. C. and Eglinton, G.: *Molecular Geochemical Indicators in Sediments*, edited by M. L. Sohn, pp. 10–32,
458 Washington, D.C., 1986.
- 459 Buckles, L. K., Weijers, J. W. H., Tran, X. M., Waldron, S. and Sinninghe Damsté, J. S.: Provenance of tetraether membrane
460 lipids in a large temperate lake (Loch Lomond, UK): Implications for glycerol dialkyl glycerol tetraether (GDGT)-based
461 palaeothermometry, *Biogeosciences*, 11(19), 5539–5563, doi:10.5194/bg-11-5539-2014, 2014.
- 462 Coard, M. A., Cousen, S. M., Cuttler, A. H., Dean, H. J., Dearing, J. A., Eglinton, T. I., Greaves, A. M., Lacey, K. P.,
463 O’Sullivan, P. E., Pickering, D. A., Rhead, M. M., Rodwell, J. K. and Simola, H.: Paleolimnological studies of annually-
464 laminated sediments in Loe Pool, Cornwall, U.K., *Hydrobiologia*, 103(1), 185–191, doi:10.1007/BF00028450, 1983.

465 Cole, J. J., Prairie, Y. T., Caraco, N. F., McDowell, W. H., Tranvik, L. J., Striegl, R. G., Duarte, C. M., Kortelainen, P.,
466 Downing, J. A., Middelburg, J. J. and Melack, J.: Plumbing the global carbon cycle: Integrating inland waters into the
467 terrestrial carbon budget, *Ecosystems*, 10(1), 171–184, doi:10.1007/s10021-006-9013-8, 2007.

468 Dang, X., Yang, H., Naafs, B. D. A., Pancost, R. D. and Xie, S.: Evidence of moisture control on the methylation of
469 branched glycerol dialkyl glycerol tetraethers in semi-arid and arid soils, *Geochim. Cosmochim. Acta*, 189, 24–36,
470 doi:10.1016/j.gca.2016.06.004, 2016.

471 Davidson, E. A. and Janssens, I. A.: Temperature sensitivity of soil carbon decomposition and feedbacks to climate change,
472 *Nature*, 440(7081), 165–173, doi:10.1038/nature04514, 2006.

473 De Jonge, C., Hopmans, E. C., Stadnitskaia, A., Rijpstra, W. I. C., Hofland, R., Tegelaar, E. and Sinninghe Damsté, J. S.:
474 Identification of novel penta- and hexamethylated branched glycerol dialkyl glycerol tetraethers in peat using HPLC–MS2,
475 GC–MS and GC–SMB-MS, *Org. Geochem.*, 54, 78–82, doi:10.1016/j.orggeochem.2012.10.004, 2013.

476 De Jonge, C., Stadnitskaia, A., Hopmans, E. C., Cherkashov, G., Fedotov, A. and Sinninghe Damsté, J. S.: In situ produced
477 branched glycerol dialkyl glycerol tetraethers in suspended particulate matter from the Yenisei River, Eastern Siberia,
478 *Geochim. Cosmochim. Acta*, 125, 476–491, doi:10.1016/j.gca.2013.10.031, 2014a.

479 De Jonge, C., Hopmans, E. C., Zell, C. I., Kim, J.-H., Schouten, S. and Sinninghe Damsté, J. S.: Occurrence and abundance
480 of 6-methyl branched glycerol dialkyl glycerol tetraethers in soils: Implications for palaeoclimate reconstruction, *Geochim.*
481 *Cosmochim. Acta*, 141, 97–112, doi:10.1016/j.gca.2014.06.013, 2014b.

482 De Jonge, C., Stadnitskaia, A., Hopmans, E. C., Cherkashov, G., Fedotov, A., Streletskaia, I. D., Vasiliev, A. A. and
483 Sinninghe Damsté, J. S.: Drastic changes in the distribution of branched tetraether lipids in suspended matter and sediments
484 from the Yenisei River and Kara Sea (Siberia): Implications for the use of brGDGT-based proxies in coastal marine
485 sediments, *Geochim. Cosmochim. Acta*, 165, 200–225, doi:10.1016/j.gca.2015.05.044, 2015.

486 Dearing Crampton-Flood, E., Peterse, F., Munsterman, D. and Sinninghe Damsté, J. S.: Using tetraether lipids archived in
487 North Sea Basin sediments to extract North Western European Pliocene continental air temperatures, *Earth Planet. Sci. Lett.*,
488 490(March), 193–205, doi:10.1016/j.epsl.2018.03.030, 2018.

489 Dirghangi, S. S., Pagani, M., Hren, M. T. and Tipple, B. J.: Distribution of glycerol dialkyl glycerol tetraethers in soils from
490 two environmental transects in the USA, *Org. Geochem.*, 59, 49–60, doi:10.1016/j.orggeochem.2013.03.009, 2013.

491 Drenovsky, R. E., Steenwerth, K. L., Jackson, L. E. and Scow, K. M.: Land use and climatic factors structure regional
492 patterns in soil microbial communities, *Glob. Ecol. Biogeogr.*, 19(1), 27–39, doi:10.1111/j.1466-8238.2009.00486.x, 2010.

493 Eglinton, G. and Hamilton, R. J.: Leaf Epicuticular Waxes, *Science* (80-.), 156(3780), 1322–1335,
494 doi:10.1126/science.156.3780.1322, 1967.

495 Feng, X., Vonk, J. E., van Dongen, B. E., Gustafsson, O., Semiletov, I. P., Dudarev, O. V., Wang, Z., Montlucon, D. B.,
496 Wacker, L. and Eglinton, T. I.: Differential mobilization of terrestrial carbon pools in Eurasian Arctic river basins, *Proc.*
497 *Natl. Acad. Sci.*, 110(35), 14168–14173, doi:10.1073/pnas.1307031110, 2013.

498 Feng, X., Feakins, S. J., Liu, Z., Ponton, C., Wang, R. Z., Karkabi, E., Galy, V., Berelson, W. M., Nottingham, A. T., Meir,
499 P. and West, A. J.: Source to sink: Evolution of lignin composition in the Madre de Dios River system with connection to the
500 Amazon basin and offshore, *J. Geophys. Res. Biogeosciences*, 121(5), 1316–1338, doi:10.1002/2016JG003323, 2016.

501 Fernandes, M. B. and Sicre, M. A.: The importance of terrestrial organic carbon inputs on Kara Sea shelves as revealed by n-
502 alkanes, OC and $\delta^{13}\text{C}$ values, *Org. Geochem.*, 31(5), 363–374, doi:10.1016/S0146-6380(00)00006-1, 2000.

503 Fierer, N. and Jackson, R. B.: The diversity and biogeography of soil bacterial communities., *Proc. Natl. Acad. Sci. U. S. A.*,
504 103(3), 626–31, doi:10.1073/pnas.0507535103, 2006.

505 Flory, J. E. and Hawley, G. R. W.: A hydrodictyon reticulatum bloom at loe pool, cornwall, *Eur. J. Phycol.*, 29(1), 17–20,
506 doi:10.1080/09670269400650431, 1994.

507 Freymond, C. V., Peterse, F., Fischer, L. V., Filip, F., Giosan, L. and Eglinton, T. I.: Branched GDGT signals in fluvial

508 sediments of the Danube River basin: Method comparison and longitudinal evolution, *Org. Geochem.*, 103, 88–96,
509 doi:10.1016/j.orggeochem.2016.11.002, 2017.

510 Glendell, M., Jones, R., Dungait, J. A. J., Meusburger, K., Schwendel, A. C., Barclay, R., Barker, S., Haley, S., Quine, T. A.
511 and Meersmans, J.: Tracing of particulate organic C sources across the terrestrial-aquatic continuum, a case study at the
512 catchment scale (Carminowe Creek, southwest England), *Sci. Total Environ.*, 616–617, 1077–1088,
513 doi:10.1016/j.scitotenv.2017.10.211, 2018.

514 Goñi, M. A., Ruttenger, K. C. and Eglinton, T. I.: Sources and contribution of terrigenous organic carbon to surface
515 sediments in the Gulf of Mexico, *Nature*, 389(6648), 275–278, doi:10.1038/38477, 1997.

516 Harvey, H. R., Fallon, R. D. and Patton, J. S.: The effect of organic matter and oxygen on the degradation of bacterial
517 membrane lipids in marine sediments, *Geochim. Cosmochim. Acta*, 50(5), 795–804, doi:10.1016/0016-7037(86)90355-8,
518 1986.

519 Hedges, J. I., Clark, W. A., Quay, P. D., Richey, J. E., Devol, A. H. and Santos, M.: Compositions and fluxes of particulate
520 organic material in the Amazon River, *Limnol. Oceanogr.*, 31(4), 717–738, doi:10.4319/lo.1986.31.4.0717, 1986.

521 Hedges, J. I., Keil, R. G. and Benner, R.: What happens to terrestrial organic matter in the ocean?, *Org. Geochem.*, 27(5–6),
522 195–212, doi:10.1016/S0146-6380(97)00066-1, 1997.

523 Hedges, J. I., Mayorga, E., Tsamakis, E., McClain, M. E., Aufdenkampe, A., Quay, P., Richey, J. E., Benner, R., Opsahl, S.,
524 Black, B., Pimentel, T., Quintanilla, J. and Maurice, L.: Organic matter in Bolivian tributaries of the Amazon River: A
525 comparison to the lower mainstream, *Limnol. Oceanogr.*, 45(7), 1449–1466, doi:10.4319/lo.2000.45.7.1449, 2000.

526 Hemingway, J. D., Schefuß, E., Spencer, R. G. M., Dinga, B. J., Eglinton, T. I., McIntyre, C. and Galy, V. V.: Hydrologic
527 controls on seasonal and inter-annual variability of Congo River particulate organic matter source and reservoir age, *Chem.*
528 *Geol.*, 466(October), 454–465, doi:10.1016/j.chemgeo.2017.06.034, 2017.

529 Hopmans, E. C., Weijers, J. W. H., Schefuß, E., Herfort, L., Sinninghe Damsté, J. S. and Schouten, S.: A novel proxy for
530 terrestrial organic matter in sediments based on branched and isoprenoid tetraether lipids, *Earth Planet. Sci. Lett.*, 224(1–2),
531 107–116, doi:10.1016/j.epsl.2004.05.012, 2004.

532 Hopmans, E. C., Schouten, S. and Sinninghe Damsté, J. S.: The effect of improved chromatography on GDGT-based
533 palaeoproxies, *Org. Geochem.*, 93, 1–6, doi:10.1016/j.orggeochem.2015.12.006, 2016.

534 Huguet, A., Meador, T. B., Laggoun-Défarge, F., Könneke, M., Wu, W., Derenne, S. and Hinrichs, K. U.: Production rates
535 of bacterial tetraether lipids and fatty acids in peatland under varying oxygen concentrations, *Geochim. Cosmochim. Acta*,
536 203, 103–116, doi:10.1016/j.gca.2017.01.012, 2017.

537 Huguet, C., Hopmans, E. C., Febo-Ayala, W., Thompson, D. H., Sinninghe Damsté, J. S. and Schouten, S.: An improved
538 method to determine the absolute abundance of glycerol dibiphytanyl glycerol tetraether lipids, *Org. Geochem.*, 37(9), 1036–
539 1041, doi:10.1016/j.orggeochem.2006.05.008, 2006.

540 Inglis, G. N., Collinson, M. E., Riegel, W., Wilde, V., Farnsworth, A., Lunt, D. J., Valdes, P., Robson, B. E., Scott, A. C.,
541 Lenz, O. K., Naafs, B. D. A. and Pancost, R. D.: Mid-latitude continental temperatures through the early Eocene in western
542 Europe, *Earth Planet. Sci. Lett.*, 460, 86–96, doi:10.1016/j.epsl.2016.12.009, 2017.

543 Jaeschke, A., Rethemeyer, J., Lappé, M., Schouten, S., Boeckx, P. and Schefuß, E.: Influence of land use on distribution of
544 soil n-alkane δD and brGDGTs along an altitudinal transect in Ethiopia: Implications for (paleo)environmental studies, *Org.*
545 *Geochem.*, 124, 77–87, doi:10.1016/j.orggeochem.2018.06.006, 2018.

546 Janzen, H. H.: Carbon cycling in earth systems - A soil science perspective, *Agric. Ecosyst. Environ.*, 104(3), 399–417,
547 doi:10.1016/j.agee.2004.01.040, 2004.

548 Kim, J. H., Zell, C., Moreira-Turcq, P., Pérez, M. A. P., Abril, G., Mortillaro, J. M., Weijers, J. W. H., Meziane, T. and
549 Sinninghe Damsté, J. S.: Tracing soil organic carbon in the lower Amazon River and its tributaries using GDGT distributions
550 and bulk organic matter properties, *Geochim. Cosmochim. Acta*, 90, 163–180, doi:10.1016/j.gca.2012.05.014, 2012.

551 Kim, J. H., Ludwig, W., Buscail, R., Dorhout, D. and Sinninghe Damsté, J. S.: Tracing tetraether lipids from source to sink
552 in the Rhône river system (NW Mediterranean), *Front. Earth Sci.*, 3(June), doi:10.3389/feart.2015.00022, 2015.

553 Liang, J., Russell, J. M., Xie, H., Lupien, R. L., Si, G., Wang, J., Hou, J. and Zhang, G.: Vegetation effects on temperature
554 calibrations of branched glycerol dialkyl glycerol tetraether (brGDGTs) in soils, *Org. Geochem.*, 127, 1–11,
555 doi:10.1016/j.orggeochem.2018.10.010, 2019.

556 Loomis, S. E., Russell, J. M. and Sinninghe Damsté, J. S.: Distributions of branched GDGTs in soils and lake sediments
557 from western Uganda: Implications for a lacustrine paleothermometer, *Org. Geochem.*, 42(7), 739–751,
558 doi:10.1016/j.orggeochem.2011.06.004, 2011.

559 Loomis, S. E., Russell, J. M., Heurreux, A. M., D'Andrea, W. J. and Sinninghe Damsté, J. S.: Seasonal variability of
560 branched glycerol dialkyl glycerol tetraethers (brGDGTs) in a temperate lake system, *Geochim. Cosmochim. Acta*, 144,
561 173–187, doi:10.1016/j.gca.2014.08.027, 2014.

562 Menges, J., Huguet, C., Alcañiz, J. M., Fietz, S., Sachse, D. and Rosell-Melé, A.: Influence of water availability in the
563 distributions of branched glycerol dialkyl glycerol tetraether in soils of the Iberian Peninsula, *Biogeosciences*, 11(10), 2571–
564 2581, doi:10.5194/bg-11-2571-2014, 2014.

565 Ménot, G., Bard, E., Rostek, F., Weijers, J. W. H., Hopmans, E. C., Schouten, S. and Sinninghe Damsté, J. S.: Early
566 Reactivation of European Rivers During the Last Deglaciation, *Science (80-.)*, 313(September), 1623–1625, 2006.

567 Miller, D. R., Helen Habicht, M., Keisling, B. A., Castañeda, I. S. and Bradley, R. S.: A 900-year New England temperature
568 reconstruction from in situ seasonally produced branched glycerol dialkyl glycerol tetraethers (brGDGTs), *Clim. Past*,
569 14(11), 1653–1667, doi:10.5194/cp-14-1653-2018, 2018.

570 Mueller-Niggemann, C., Utami, S. R., Marxen, A., Mangelsdorf, K., Bauersachs, T. and Schwark, L.: Distribution of
571 tetraether lipids in agricultural soils – differentiation between paddy and upland management,
572 *Biogeosciences*, 13(5), 1647–1666, doi:10.5194/bg-13-1647-2016, 2016.

573 Naafs, B. D. A., Inglis, G. N., Zheng, Y., Amesbury, M. J., Biester, H., Bindler, R., Blewett, J., Burrows, M. A., del Castillo
574 Torres, D., Chambers, F. M., Cohen, A. D., Evershed, R. P., Feakins, S. J., Galka, M., Gallego-Sala, A., Gandois, L., Gray,
575 D. M., Hatcher, P. G., Honorio Coronado, E. N., Hughes, P. D. M., Huguet, A., Könönen, M., Laggoun-Défarge, F.,
576 Lähteenoja, O., Lamentowicz, M., Marchant, R., McClymont, E., Pontevedra-Pombal, X., Ponton, C., Pourmand, A.,
577 Rizzuti, A. M., Rochefort, L., Schellekens, J., De Vleeschouwer, F. and Pancost, R. D.: Introducing global peat-specific
578 temperature and pH calibrations based on brGDGT bacterial lipids, *Geochim. Cosmochim. Acta*, 208(June 2016), 285–301,
579 doi:10.1016/j.gca.2017.01.038, 2017.

580 Naeher, S., Peterse, F., Smittenberg, R. H., Niemann, H., Zigah, P. K. and Schubert, C. J.: Sources of glycerol dialkyl
581 glycerol tetraethers (GDGTs) in catchment soils, water column and sediments of Lake Rotsee (Switzerland) - Implications
582 for the application of GDGT-based proxies for lakes, *Org. Geochem.*, 66, 164–173, doi:10.1016/j.orggeochem.2013.10.017,
583 2014.

584 O'Sullivan, P. E. and West, P. S.: understanding and recommendations for restoration , based on , 421–434, 1992.

585 Peterse, F., Kim, J. H., Schouten, S., Kristensen, D. K., Koç, N. and Sinninghe Damsté, J. S.: Constraints on the application
586 of the MBT/CBT palaeothermometer at high latitude environments (Svalbard, Norway), *Org. Geochem.*, 40(6), 692–699,
587 doi:10.1016/j.orggeochem.2009.03.004, 2009.

588 Peterse, F., Nicol, G. W., Schouten, S. and Sinninghe Damsté, J. S.: Influence of soil pH on the abundance and distribution
589 of core and intact polar lipid-derived branched GDGTs in soil, *Org. Geochem.*, 41(10), 1171–1175,
590 doi:10.1016/j.orggeochem.2010.07.004, 2010.

591 Peterse, F., Prins, M. A., Beets, C. J., Troelstra, S. R., Zheng, H., Gu, Z., Schouten, S. and Damsté, J. S. S.: Decoupled
592 warming and monsoon precipitation in East Asia over the last deglaciation, *Earth Planet. Sci. Lett.*, 301(1–2), 256–264,
593 doi:10.1016/j.epsl.2010.11.010, 2011.

594 Peterse, F., van der Meer, J., Schouten, S., Weijers, J. W. H., Fierer, N., Jackson, R. B., Kim, J. H. and Sinninghe Damsté, J.
595 S.: Revised calibration of the MBT-CBT paleotemperature proxy based on branched tetraether membrane lipids in surface
596 soils, *Geochim. Cosmochim. Acta*, 96, 215–229, doi:10.1016/j.gca.2012.08.011, 2012.

597 Powers, L. A., Werne, J. P., Johnson, T. C., Hopmans, E. C., Sinninghe Damsté, J. S. and Schouten, S.: Crenarchaeotal
598 membrane lipids in lake sediments: A new paleotemperature proxy continental paleoclimate reconstruction?, *Geology*,
599 32(7), 613–616, doi:10.1130/G20434.1, 2004.

600 R Core Team, R: A language and environment for statistical computing, <http://www.R-project.org>, 2018.

601 Russell, J. M., Hopmans, E. C., Loomis, S. E., Liang, J. and Sinninghe Damsté, J. S.: Distributions of 5- and 6-methyl
602 branched glycerol dialkyl glycerol tetraethers (brGDGTs) in East African lake sediment: Effects of temperature, pH, and
603 new lacustrine paleotemperature calibrations, *Org. Geochem.*, 117, 56–69, doi:10.1016/j.orggeochem.2017.12.003, 2018.

604 Schoon, P. L., De Kluijver, A., Middelburg, J. J., Downing, J. A., Sinninghe Damsté, J. S. and Schouten, S.: Influence of
605 lake water pH and alkalinity on the distribution of core and intact polar branched glycerol dialkyl glycerol tetraethers
606 (GDGTs) in lakes, *Org. Geochem.*, 60, 72–82, doi:10.1016/j.orggeochem.2013.04.015, 2013.

607 Schouten, S., Hopmans, E. C., Pancost, R. D. and Sinninghe Damsté, J. S.: Widespread occurrence of structurally diverse
608 tetraether membrane lipids: Evidence for the ubiquitous presence of low-temperature relatives of hyperthermophiles, *Proc.*
609 *Natl. Acad. Sci.*, 97(26), 14421–14426, doi:10.1073/pnas.97.26.14421, 2000.

610 Sinninghe Damsté, J. S., Schouten, S., Hopmans, E. C., van Duin, A. C. T. and Geenevasen, J. A. J.: Crenarchaeol, *J. Lipid*
611 *Res.*, 43(10), 1641–1651, doi:10.1194/jlr.M200148-JLR200, 2002.

612 Sinninghe Damsté, J. S., Ossebaar, J., Abbas, B., Schouten, S. and Verschuren, D.: Fluxes and distribution of tetraether
613 lipids in an equatorial African lake: Constraints on the application of the TEX86 palaeothermometer and BIT index in
614 lacustrine settings, *Geochim. Cosmochim. Acta*, 73(14), 4232–4249, doi:10.1016/j.gca.2009.04.022, 2009.

615 Sinninghe Damsté, J. S., Rijpstra, W. I. C., Hopmans, E. C., Weijers, J. W. H., Foessel, B. U., Overmann, J. and Dedysh, S.
616 N.: 13,16-Dimethyl octacosanedioic acid (iso-Diabolic Acid), a common membrane-spanning lipid of Acidobacteria
617 subdivisions 1 and 3, *Appl. Environ. Microbiol.*, 77(12), 4147–4154, doi:10.1128/AEM.00466-11, 2011.

618 Sinninghe Damsté, J. S., Rijpstra, W. I. C., Hopmans, E. C., Foessel, B. U., Wüst, P. K., Overmann, J., Tank, M., Bryant, D.
619 A., Dunfield, P. F., Houghton, K. and Stott, M. B.: Ether- and ester-bound iso-diabolic acid and other lipids in members of
620 Acidobacteria subdivision 4, *Appl. Environ. Microbiol.*, 80(17), 5207–5218, doi:10.1128/AEM.01066-14, 2014.

621 Sinninghe Damsté, J. S.: Spatial heterogeneity of sources of branched tetraethers in shelf systems: The geochemistry of
622 tetraethers in the Berau River delta (Kalimantan, Indonesia), *Geochim. Cosmochim. Acta*, 186, 13–31,
623 doi:10.1016/j.gca.2016.04.033, 2016.

624 Sinninghe Damsté, J. S., Rijpstra, W. I. C., Foessel, B. U., Huber, K. J., Overmann, J., Nakagawa, S., Kim, J. J., Dunfield, P.
625 F., Dedysh, S. N. and Villanueva, L.: An overview of the occurrence of ether- and ester-linked iso-diabolic acid membrane
626 lipids in microbial cultures of the Acidobacteria: Implications for brGDGT paleoproxies for temperature and pH, *Org.*
627 *Geochem.*, 124, 63–76, doi:10.1016/j.orggeochem.2018.07.006, 2018.

628 Smith, P.: Land use change and soil organic carbon dynamics, *Nutr. Cycl. Agroecosystems*, 81(2), 169–178,
629 doi:10.1007/s10705-007-9138-y, 2008.

630 Steenwerth, K. L., Jackson, L. E., Calderón, F. J., Stromberg, M. R. and Scow, K. M.: Erratum: Soil community composition
631 and land use history in cultivated and grassland ecosystems of coastal California (*Soil Biology and Biochemistry* 34:11
632 (1599-1611)), *Soil Biol. Biochem.*, 35(3), 487–500, doi:10.1016/S0038-0717(03)00027-0, 2003.

633 Tierney, J. E. and Russell, J. M.: Distributions of branched GDGTs in a tropical lake system: Implications for lacustrine
634 application of the MBT/CBT paleoproxy, *Org. Geochem.*, 40(9), 1032–1036, doi:10.1016/j.orggeochem.2009.04.014, 2009.

635 Tierney, J. E., Russell, J. M., Eggermont, H., Hopmans, E. C., Verschuren, D. and Sinninghe Damsté, J. S.: Environmental
636 controls on branched tetraether lipid distributions in tropical East African lake sediments, *Geochim. Cosmochim. Acta*,

637 74(17), 4902–4918, doi:10.1016/j.gca.2010.06.002, 2010.

638 Wakeham, S. G. and Lee, C.: *Organic Geochemistry*, edited by M. H. Engel and S. A. Macko, Springer US, Boston, MA.,
639 1993.

640 Wang, H., Liu, W., Zhang, C. L., Liu, Z. and He, Y.: Branched and isoprenoid tetraether (BIT) index traces water content
641 along two marsh-soil transects surrounding Lake Qinghai: Implications for paleo-humidity variation, *Org. Geochem.*, 59,
642 75–81, doi:10.1016/j.orggeochem.2013.03.011, 2013.

643 Weber, Y., De Jonge, C., Rijpstra, W. I. C., Hopmans, E. C., Stadnitskaia, A., Schubert, C. J., Lehmann, M. F., Sinninghe
644 Damsté, J. S. and Niemann, H.: Identification and carbon isotope composition of a novel branched GDGT isomer in lake
645 sediments: Evidence for lacustrine branched GDGT production, *Geochim. Cosmochim. Acta*, 154, 118–129,
646 doi:10.1016/j.gca.2015.01.032, 2015.

647 Weber, Y., Sinninghe Damsté, J. S., Zopfi, J., De Jonge, C., Gilli, A., Schubert, C. J., Lepori, F., Lehmann, M. F. and
648 Niemann, H.: Redox-dependent niche differentiation provides evidence for multiple bacterial sources of glycerol tetraether
649 lipids in lakes, *Proc. Natl. Acad. Sci.*, 115(43), 10926–10931, doi:10.1073/pnas.1805186115, 2018.

650 Weijers, J. W. H., Schouten, S., Hopmans, E. C., Geenevasen, J. A. J., David, O. R. P., Coleman, J. M., Pancost, R. D. and
651 Sinninghe Damsté, J. S.: Membrane lipids of mesophilic anaerobic bacteria thriving in peats have typical archaeal traits,
652 *Environ. Microbiol.*, 8(4), 648–657, doi:10.1111/j.1462-2920.2005.00941.x, 2006a.

653 Weijers, J. W. H., Schouten, S., Spaargaren, O. C. and Sinninghe Damsté, J. S.: Occurrence and distribution of tetraether
654 membrane lipids in soils: Implications for the use of the TEX86 proxy and the BIT index, *Org. Geochem.*, 37(12), 1680–
655 1693, doi:10.1016/j.orggeochem.2006.07.018, 2006b.

656 Weijers, J. W. H., Schouten, S., van den Donker, J. C., Hopmans, E. C. and Sinninghe Damsté, J. S.: Environmental controls
657 on bacterial tetraether membrane lipid distribution in soils, *Geochim. Cosmochim. Acta*, 71(3), 703–713,
658 doi:10.1016/j.gca.2006.10.003, 2007a.

659 Weijers, J. W. H., Schefuß, E., Schouten, S. and Sinninghe Damsté, J. S.: Evolution of Tropical Africa over the Last
660 Deglaciation, *Science* (80-.), 8247(March), 5–8, 2007b.

661 Weijers, J. W. H., Wiesenberg, G. L. B., Bol, R., Hopmans, E. C. and Pancost, R. D.: Carbon isotopic composition of
662 branched tetraether membrane lipids in soils suggest a rapid turnover and a heterotrophic life style of their source
663 organism(s), *Biogeosciences*, 7(9), 2959–2973, doi:10.5194/bg-7-2959-2010, 2010.

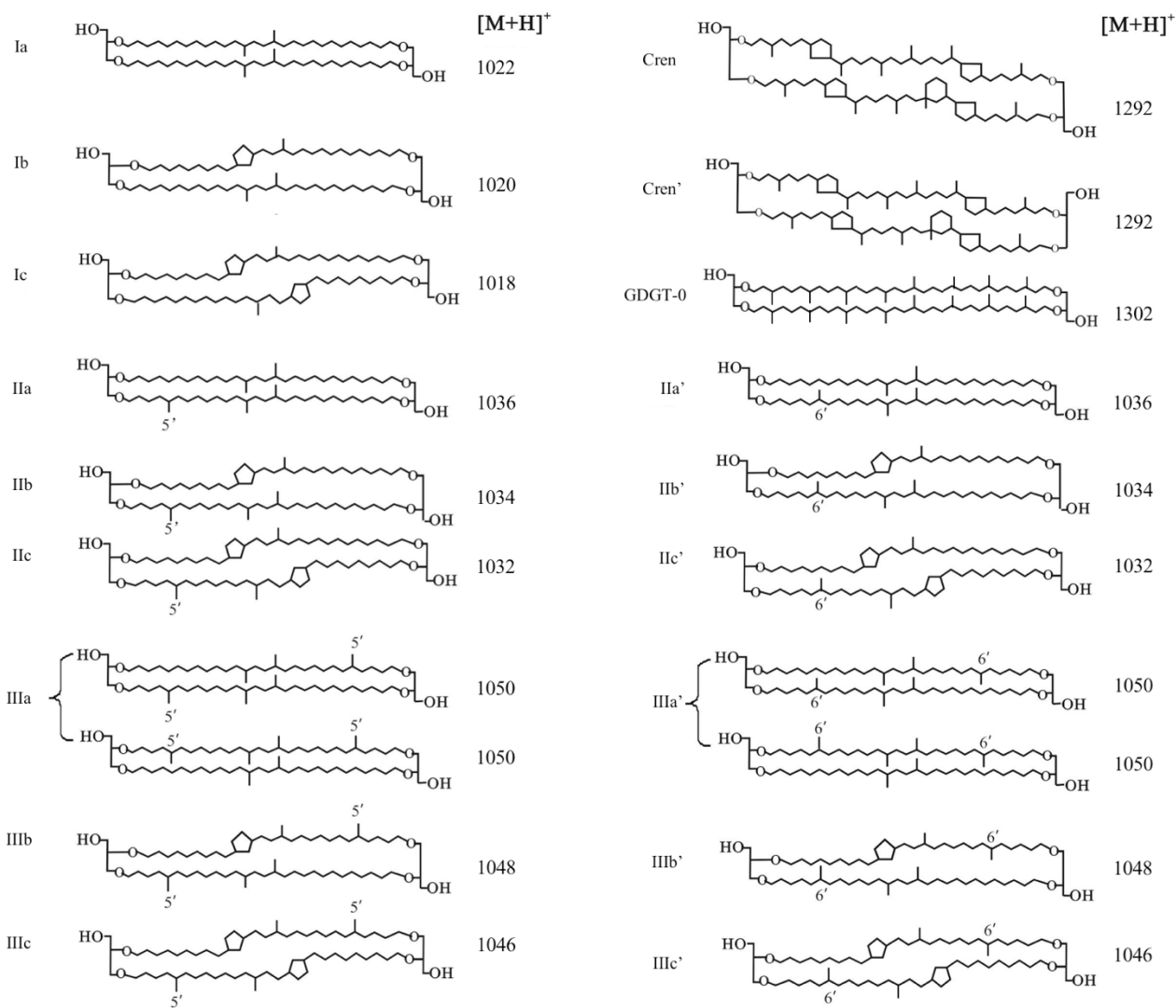
664 Weijers, J. W. H., Bernhardt, B., Peterse, F., Werne, J. P., Dungait, J. A. J., Schouten, S. and Sinninghe Damsté, J. S.:
665 Absence of seasonal patterns in MBT-CBT indices in mid-latitude soils, *Geochim. Cosmochim. Acta*, 75(11), 3179–3190,
666 doi:10.1016/j.gca.2011.03.015, 2011.

667 Zell, C., Kim, J. H., Moreira-Turcq, P., Abril, G., Hopmans, E. C., Bonnet, M. P., Sobrinho, R. L. and Sinninghe Damsté, J.
668 S.: Disentangling the origins of branched tetraether lipids and crenarchaeol in the lower Amazon river: Implications for
669 GDGT-based proxies, *Limnol. Ocean.*, 58(1), 343–353, doi:10.4319/lo.2013.58.1.0343, 2013.

670 Zell, C., Kim, J. H., Hollander, D., Lorenzoni, L., Baker, P., Silva, C. G., Nittrouer, C. and Sinninghe Damsté, J. S.: Sources
671 and distributions of branched and isoprenoid tetraether lipids on the Amazon shelf and fan: Implications for the use of
672 GDGT-based proxies in marine sediments, *Geochim. Cosmochim. Acta*, 139, 293–312, doi:10.1016/j.gca.2014.04.038,
673 2014.

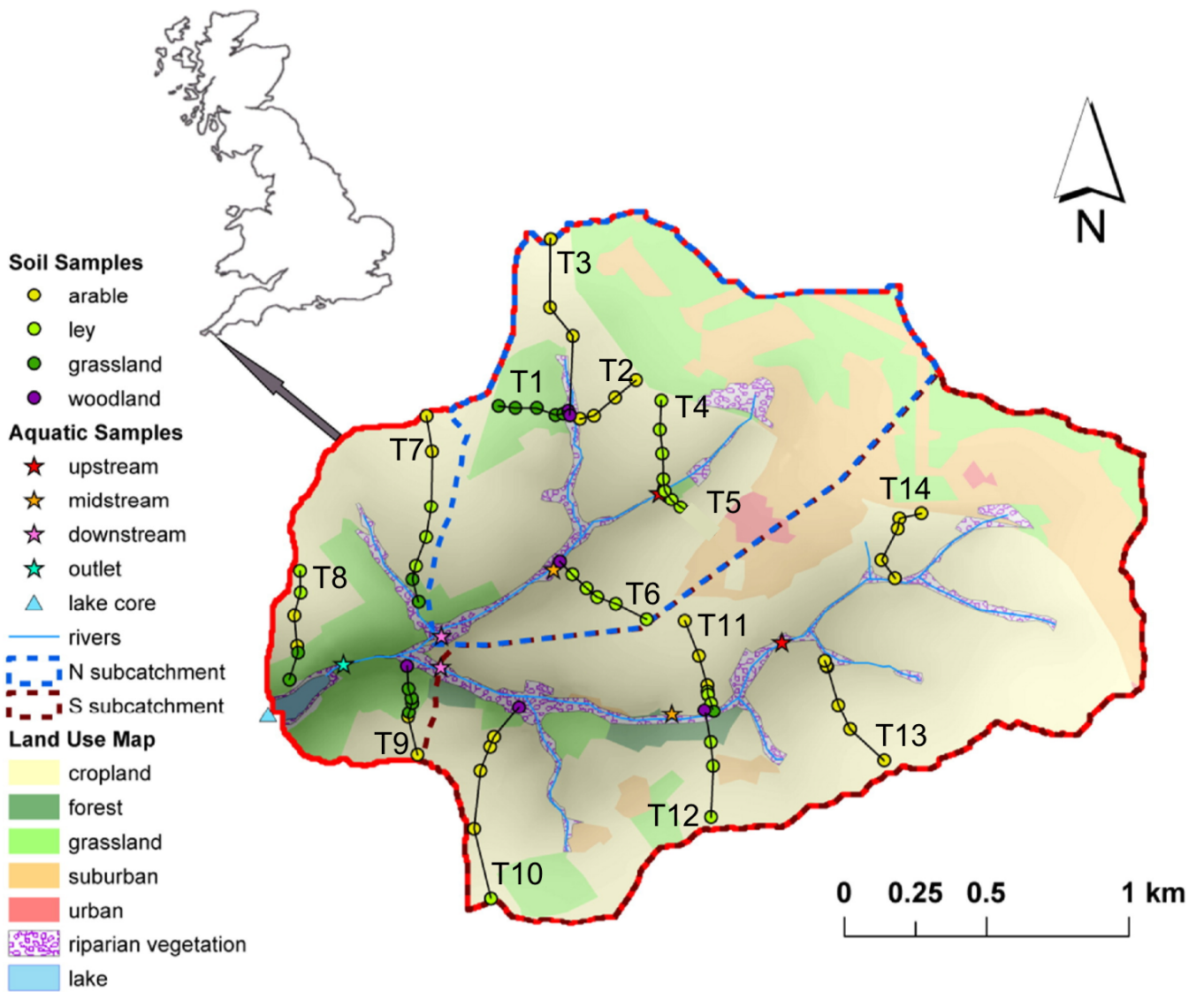
674 Zhang, C. L., Wang, J., Wei, Y., Zhu, C., Huang, L. and Dong, H.: Production of branched tetraether lipids in the lower
675 Pearl River and estuary: Effects of extraction methods and impact on bGDGT proxies, *Front. Microbiol.*, 2(JAN), 1–18,
676 doi:10.3389/fmicb.2011.00274, 2012.

677 Zheng, Y., Pancost, R. D., Liu, X., Wang, Z., Naafs, B. D. A., Xie, X., Liu, Z., Yu, X. and Yang, H.: Atmospheric
678 connections with the North Atlantic enhanced the deglacial warming in northeast China, *Geology*, 45(11), 1031–1034,
679 doi:10.1130/G39401.1, 2017.



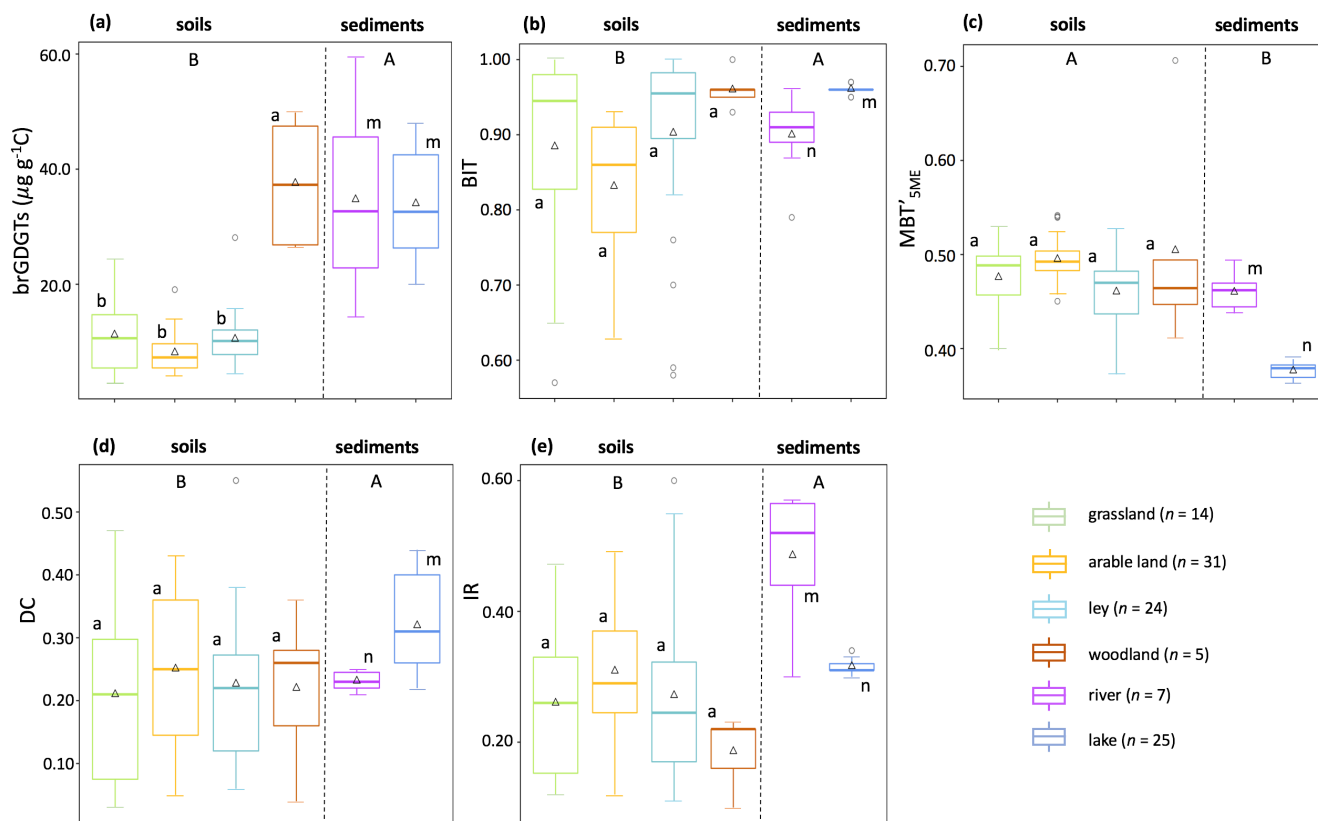
682

683 **Figure 1: Molecular structures of 5-methyl and 6-methyl branched GDGTs, GDGT-0 and crenarchaeol. The 6-methyl brGDGTs**
 684 **are represented by apostrophe. The structures of penta- and hexamethylated brGDGTs with cyclopentane moiety(ies) IIb', IIc',**
 685 **IIIb', IIIc' are tentative.**



686

687 **Figure 2: Map of the Carminowe Creek catchment in southwest England showing land use types, 14 soil transects (labelled T1-14),**
 688 **creek bed and lake core sediment sampling locations. The coloured circles and stars indicate soil samples under different land use**
 689 **types and creek bed sediments along the streams, respectively. Adjusted from Glendell et al. (2018).**



690

691

692

693

694

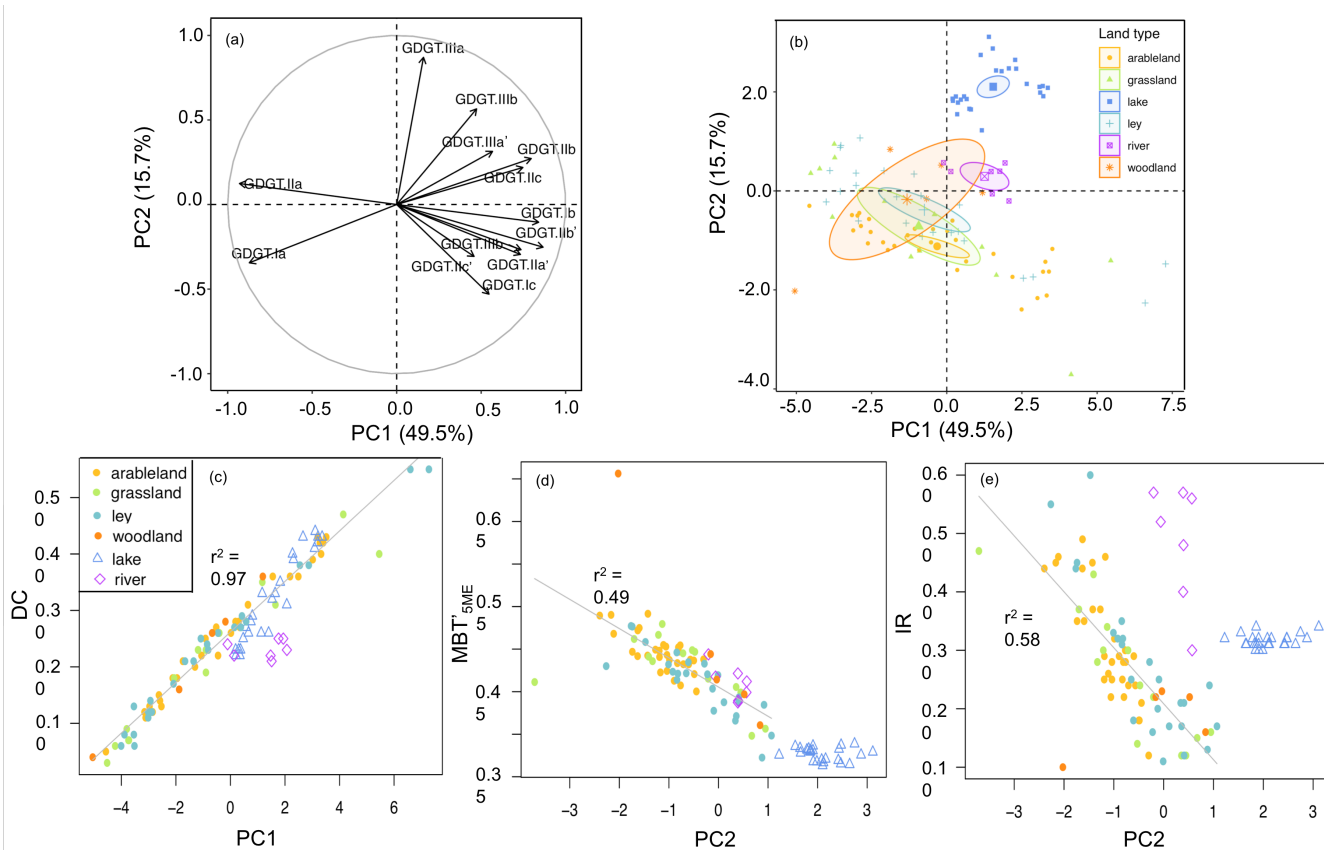
695

696

697

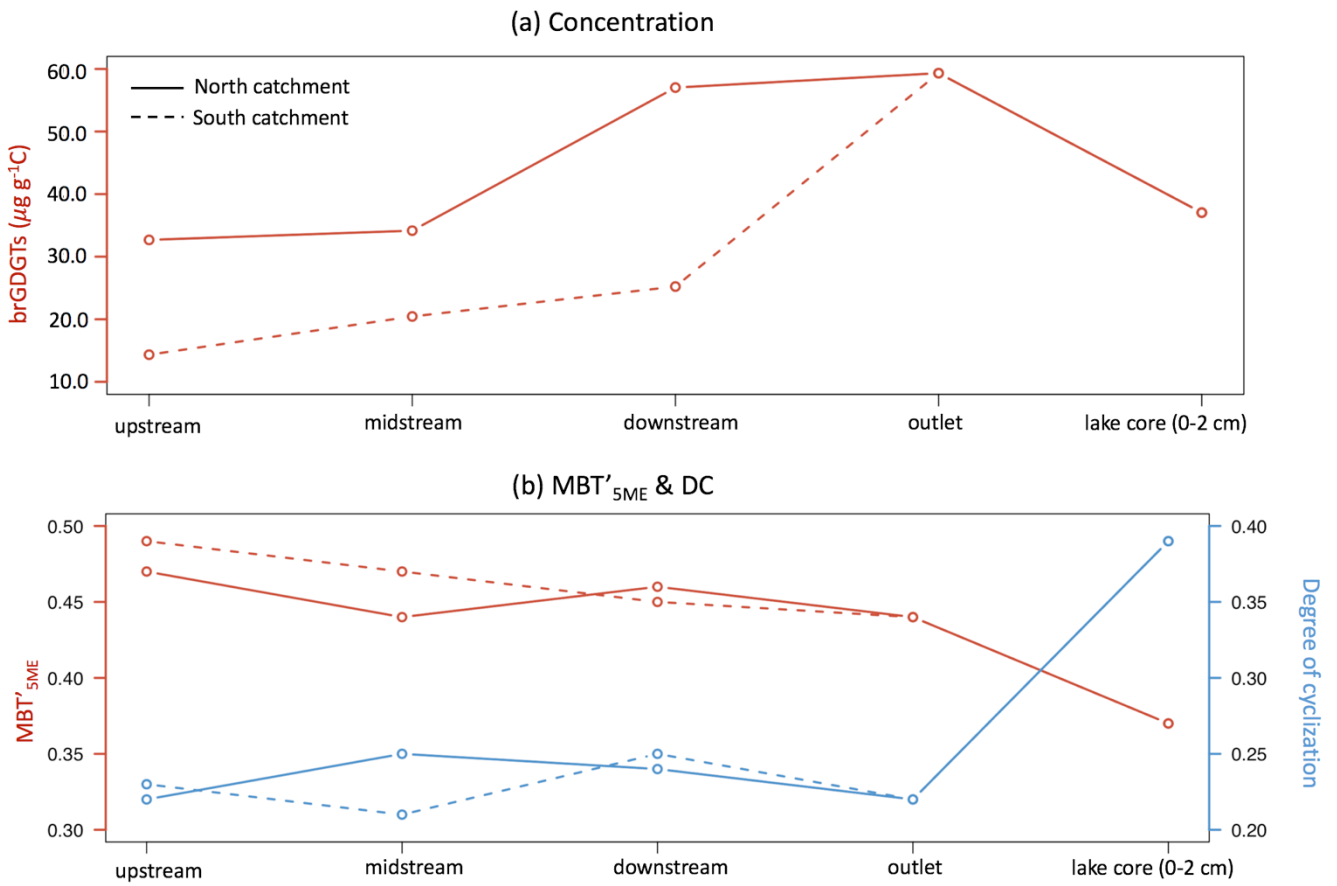
698

Figure 3: Box plots displaying (a) the C-normalized concentration of brGDGTs, and brGDGT-based proxies: (b) BIT index (branched and isoprenoid tetraether ratio), (c) $\text{MBT}'_{5\text{ME}}$ (methylation of 5-methyl branched tetraethers), (d) DC (degree of cyclisation) and (e) IR (isomerization ratio). The triangles represent the average values, the bold line indicates the median (50th percentile), bottom and top of the box indicate first quartile (25th percentile) and third quartile (75th percentile) respectively, whiskers cover the smallest and largest value within 1.5 times of the interquartile range (i.e. the distance between the top and bottom of the box). Any data points outside the whiskers are considered as outliers. Different letters indicate differences between samples: A and B for differences between catchment soils and aquatic sediments, a and b for soils under different vegetation types, and m and n for creek bed and lake core sediments ($p < 0.05$).



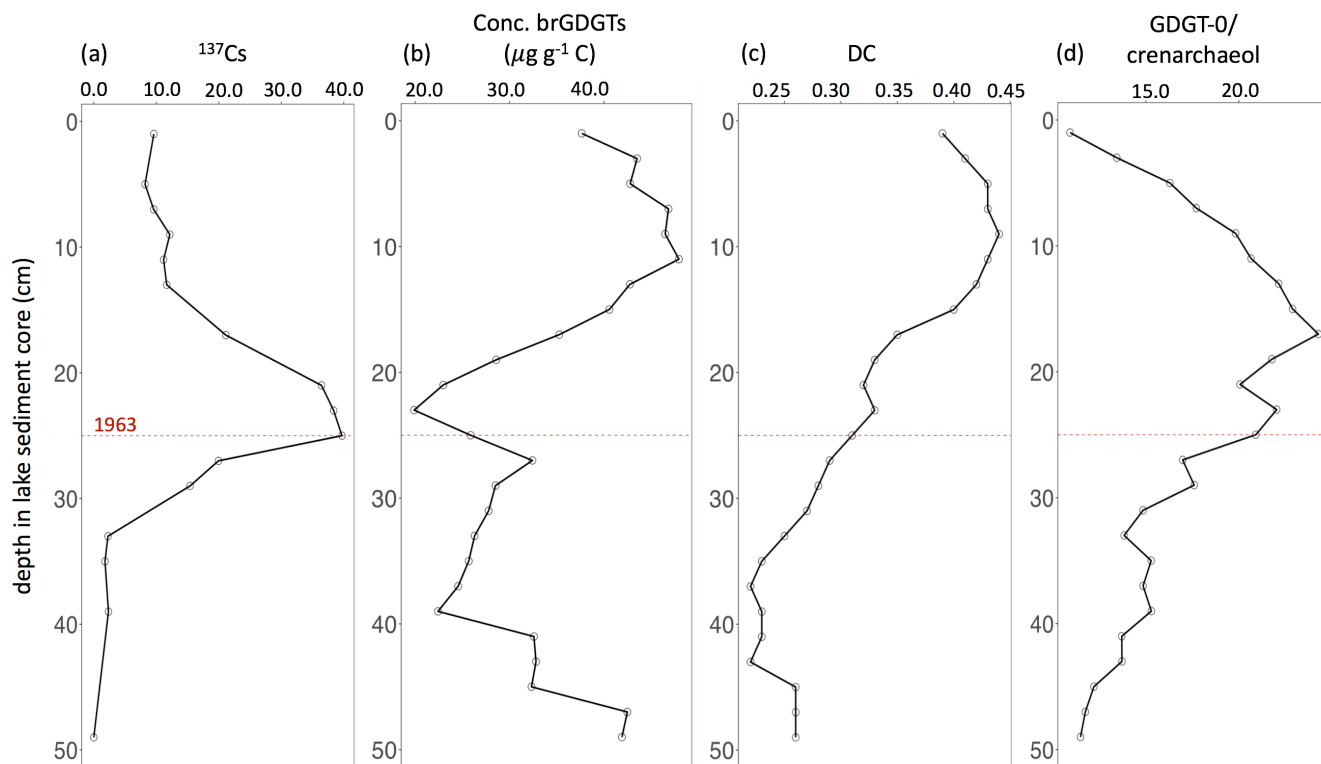
699

700 **Figure 4: PCA based on the relative abundances of 13 major brGDGTs. Figure (a) shows the distribution of 13 brGDGTs**
 701 **(brGDGT-IIIc and brGDGT-IIIc' are excluded as they are below the detection limit) along the first two PCs, roman numerals and**
 702 **English alphabet represent the compounds shown in Fig. 1. Figure (b) shows sampling sites loading scores on the first two PCs and**
 703 **95% confidence interval ellipses surrounding the mean point of different groups of land use: arable land ($n = 31$), grassland ($n =$**
 704 **14), ley ($n = 24$) and woodland ($n = 5$), and creek ($n = 7$) and lake ($n = 25$). Figure (c) shows cross plots between PC1 and DC**
 705 **(degree of cyclisation). Figure (d) and (e) show cross plots of PC2 with MBT'_{5ME} (methylation of 5-methyl branched tetraethers)**
 706 **and IR (isomerization ratio) respectively. The linear correlation was calculated excluding creek and lake sediment.**



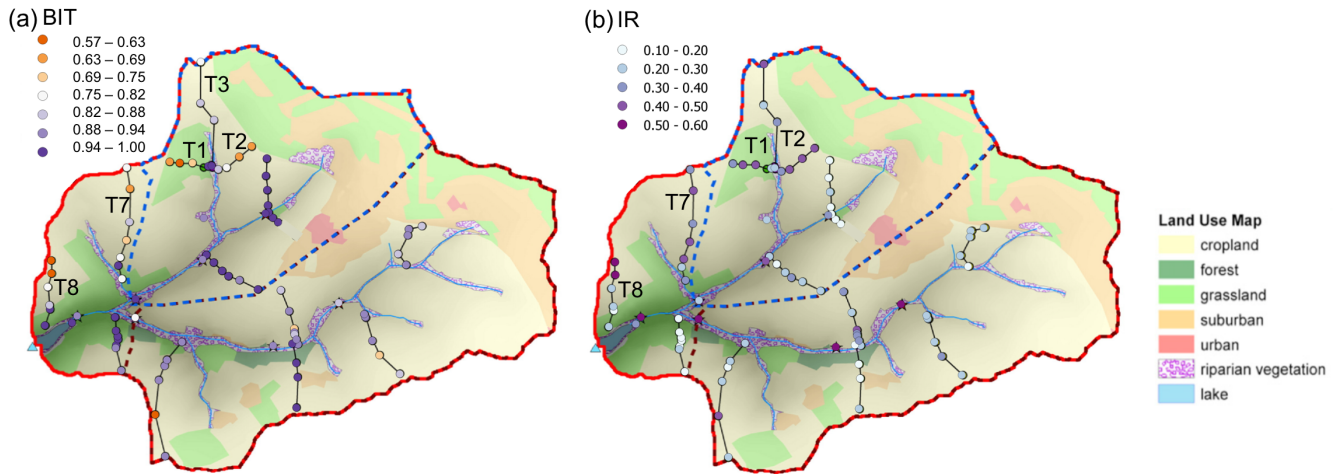
707

708 **Figure 5: Spatial variability of (a) C-normalized concentration of brGDGTs and (b) MBT'_{5ME} (methylation of 5-methyl branched**
 709 **tetraethers) and DC (degree of cyclisation) in downstream direction of both substreams in the Carminowe Creek catchment.**



710

711 **Figure 6: Lake sediment core profiles of (a) ^{137}Cs to date, (b) C-normalized concentration of brGDGTs, (c) DC (degree of**
 712 **cyclisation) and (d) ratio between GDGT-0 and crenarchaeol. The red dashed line indicates the year of 1963.**



713

714 Appendix Fig.1: Spatial variability of the (a) BIT (branched and isoprenoid tetraether ratio) and (b) IR (isomerization ratio) along
 715 14 soil transects in the Carminowe Creek catchment. The coloured circles show the concentrations and proxy values. Tx indicates
 716 soil transects discussed in the text. The background colours indicate different land use types. Adjusted from Glendell et al. (2018).

Table 1. C% (carbon content), pH values, average concentrations of brGDGTs and brGDGT-based proxies under different land use types. BIT (branched and isoprenoid tetraether ratio), MBT_{5ME} (methylation of 5-methyl branched tetraethers), %tetra (percentage of tetramethylated brGDGTs), %penta (percentage of pentamethylated brGDGTs), %hexa (percentage of hexamethylated brGDGTs), DC (degree of cyclisation), IR (isomerization ratio) (mean \pm standard deviation, s.d.).

Land use (n)	C% *	pH	Conc. ($\mu\text{g g}^{-1}$ soil)	Conc. ($\mu\text{g g}^{-1}$ C)	BIT	MBT _{5ME}	%tetra	%penta	%hexa	DC	IR
arable (31)	2.9 \pm 0.5	6.6 \pm 0.4	0.2 \pm 0.1	8.1 \pm 3.6	0.83 \pm 0.09	0.50 \pm 0.02	40.1 \pm 3.1	49.7 \pm 1.5	10.2 \pm 1.8	0.25 \pm 0.11	0.31 \pm 0.10
grass (14)	5.6 \pm 1.2	6.0 \pm 0.5	0.6 \pm 0.4	11.2 \pm 6.7	0.88 \pm 0.14	0.48 \pm 0.04	39.8 \pm 4.0	49.4 \pm 2.3	10.8 \pm 2.1	0.21 \pm 0.14	0.26 \pm 0.12
ley (24)	3.6 \pm 0.9	6.0 \pm 0.3	0.4 \pm 0.3	10.5 \pm 4.8	0.90 \pm 0.12	0.46 \pm 0.04	37.8 \pm 3.7	50.2 \pm 2.0	12.0 \pm 2.9	0.23 \pm 0.14	0.27 \pm 0.13
woodland (5)	8.2 \pm 2.1	5.4 \pm 0.7	3.0 \pm 1.0	37.6 \pm 11.0	0.96 \pm 0.03	0.50 \pm 0.12	45.4 \pm 13.0	44.4 \pm 8.3	10.3 \pm 4.8	0.22 \pm 0.12	0.19 \pm 0.05
all soils (74)	4.0 \pm 1.8	6.2 \pm 0.5	0.6 \pm 0.8	11.5 \pm 8.9	0.87 \pm 0.12	0.48 \pm 0.04	39.7 \pm 4.9	49.4 \pm 3.0	10.9 \pm 2.6	0.23 \pm 0.13	0.28 \pm 0.11
creek (7)	2.3 \pm 0.8	7.1 \pm 0.2	0.8 \pm 0.4	34.7 \pm 17.4	0.90 \pm 0.06	0.46 \pm 0.02	30.1 \pm 4.5	45.0 \pm 0.7	24.9 \pm 4.7	0.23 \pm 0.02	0.48 \pm 0.10
Lake (25)	7.5 \pm 1.0	5.7 \pm 0.2	2.6 \pm 0.7	34.0 \pm 8.7	0.96 \pm 0.01	0.38 \pm 0.01	28.9 \pm 0.7	50.2 \pm 1.8	21.0 \pm 1.4	0.32 \pm 0.08	0.32 \pm 0.01

717 *From Glendell et al. (2018)

Appendix Table 1. BIT values along 14 transects (Tx indicates the transect number, and Sx indicates the sample point, where 1 represents the hilltop and subsequent numbers are further downslope).

	BIT	North catchment								South catchment					
		T1	T2	T3	T4	T5	T6	T7	T8	T9	T10	T11	T12	T13	T14
hilltop	S1	0.65	<i>0.66</i>	<i>0.77</i>	0.97	0.99	0.97	<i>0.77</i>	0.58	0.92	0.92	0.84	0.95	0.84	0.86
	S2	0.57	<i>0.66</i>	<i>0.86</i>	0.99	0.99	0.93	<i>0.65</i>	0.59	0.91	0.63	-	-	0.73	0.88
	S3	0.73	<i>0.77</i>	<i>0.87</i>	1.00	1.00	0.94	<i>0.82</i>	0.80	0.98	0.90	0.92	0.98	0.91	0.88
	S4	0.88	<i>0.83</i>	<i>0.96</i>	0.99	-	0.96	<i>0.70</i>	0.85	1.00	0.92	0.72	0.98	0.92	0.86
	S5	0.95	-	-	-	-	0.97	<i>0.76</i>	0.98	1.00	0.91	0.91	1.00	0.91	0.93
	S6	-	-	-	-	-	0.96	<i>0.94</i>	0.97	1.00	0.93	0.85	-	0.90	-
	S7	-	-	-	-	-	-	<i>0.81</i>	-	0.95	-	0.92	-	-	-
downslope	S8	-	-	-	-	-	-	-	-	-	-	0.92	-	-	-

718